Article

Golgi maturation-dependent glycoenzyme recycling controls glycosphingolipid biosynthesis and cell growth via GOLPH3

Riccardo Rizzo[1,2,*,†] (iD), Domenico Russo[1,†] (iD), Kazuo Kurokawa[3], Pranoy Sahu[1], Bernadette Lombardi[1], Domenico Supino[1], Mikhail A Zhukovsky[1], Anthony Vocat[4], Prathyush Pothukuchi[1], Vidya Kunnathully[1], Laura Capolupo[4], Gaelle Boncompain[5] (iD), Carlo Vitagliano[6] (iD), Federica Zito Marino[6], Gabriella Aquino[6], Daniela Montariello[1], Petra Henklein[7], Luigi Mandrich[1], Gerardo Botti[6], Henrik Clausen[8] (iD), Ulla Mandel[8], Toshiyuki Yamaji[9], Kentaro Hanada[9] (iD), Alfredo Budillon[6], Franck Perez[5] (iD), Seetharaman Parashuraman[1] (iD), Yusuf A Hannun[10] (iD), Akihiko Nakano[3] (iD), Daniela Corda[1] (iD), Giovanni D'Angelo[1,4,**,‡] (iD) & Alberto Luini[1,***,‡] (iD)

Abstract

Glycosphingolipids are important components of the plasma membrane where they modulate the activities of membrane proteins including signalling receptors. Glycosphingolipid synthesis relies on competing reactions catalysed by Golgi-resident enzymes during the passage of substrates through the Golgi cisternae. The glycosphingolipid metabolic output is determined by the position and levels of the enzymes within the Golgi stack, but the mechanisms that coordinate the intra-Golgi localisation of the enzymes are poorly understood. Here, we show that a group of sequentially-acting enzymes operating at the branchpoint among glycosphingolipid synthetic pathways binds the Golgi-localised oncoprotein GOLPH3. GOLPH3 sorts these enzymes into vesicles for intra-Golgi retro-transport, acting as a component of the cisternal maturation mechanism. Through these effects, GOLPH3 controls the sub-Golgi localisation and the lysosomal degradation rate of specific enzymes. Increased GOLPH3 levels, as those observed in tumours, alter glycosphingolipid synthesis and plasma membrane composition thereby promoting mitogenic signalling and cell proliferation. These data have medical implications as they outline a novel oncogenic mechanism of action for GOLPH3 based on glycosphingolipid metabolism.

Introduction

Glycosphingolipids (GSLs) are important components of the external leaflet of the plasma membrane (PM) where they modulate the activities of many PM proteins including signalling receptors (Hakomori, 2008; Merrill, 2011; D'Angelo *et al*, 2013a; Russo *et al*, 2016). Several aspects of GSL physiology, including GSL structure and bioactivity as well as the catalytic properties and expression patterns

1 Institute of Biochemistry and Cell Biology, National Research Council, Naples, Italy
2 Institute of Nanotechnology, National Research Council (CNR-NANOTEC), Lecce, Italy
3 Live Cell Super-Resolution Imaging Research Team, RIKEN Center for Advanced Photonics, Saitama, Japan
4 École Polytechnique Fédérale de Lausanne (EPFL), Lausanne, Switzerland
5 Institute Curie – CNRS UMR1 44, Research Center, Paris, France
6 Istituto Nazionale Tumori Fondazione G. Pascale-IRCCS, Naples, Italy
7 Humboldt-Universität zu Berlin, and Berlin Institute of Health, Institute of Biochemistry, Charité – Universitätsmedizin Berlin, corporate member of Freie Universität Berlin, Berlin, Germany
8 Faculty of Health Sciences, Centre for Glycomics, Department of Cellular and Molecular Medicine Nørre Alle 20, University of Copenhagen, Copenhagen N, Denmark
9 Department of Biochemistry & Cell Biology, National Institute of Infectious Diseases, Tokyo, Japan
10 Stony Brook University Medical Center, New York, NY, USA
*Corresponding author. Tel: +39 0832 319816; E-mail: riccardo.rizzo@nanotec.cnr.it
**Corresponding author. Tel: +41 21 693 42 76; E-mail: giovanni.dangelo@epfl.ch
***Corresponding author. Tel: +39 081 6132722; E-mail: alberto.luini@ibbc.cnr.it
†These authors contributed equally to this work
‡These authors contributed equally to this work

of GSL metabolic enzymes, are well known in principle (Merrill, 2011). Yet, our understanding of GSL biology is compromised by the lack of insight into the mechanisms by which these lipids are synthesised within the Golgi complex (D'Angelo *et al*, 2013a). Here, we aim to analyse such mechanisms.

GSL biosynthesis is template-independent and occurs during transport through the Golgi *cisternae* (Merrill, 2011) via the progressive assembly of sugar chains on the ceramide backbone by sugar transferring enzymes (glycoenzymes), organised in competing metabolic pathways (Merrill, 2011). Given this synthetic modality, GSL biosynthesis depends to a large extent on the order of the sugar addition (glycosylation) reactions (Merrill, 2011). This, in turn, depends on the distribution of the synthetic enzymes (and of accessory proteins such as sugar and ion transporters) throughout the various *cisternae* of the Golgi stack, which serve as independent reaction chambers (Pothukuchi *et al*, 2019). Thus, the intra-Golgi transport mechanisms that control the position of GSL synthetic enzymes in the stack are a key determinant of the final GSL metabolic output which, usually, consists of a limited set of cell-specific GSLs (D'Angelo *et al*, 2013a).

As schematised in Fig EV1A, GSL synthesis starts with the production of ceramide (Cer) by ceramide synthases (CerS1-6) on the cytosolic aspects of the endoplasmic reticulum (ER) membranes (Levy & Futerman, 2010). Cer is then either transported to the *trans* Golgi/*trans* Golgi network (TGN) by the lipid transfer protein CERT (Hanada *et al*, 2003) for production of sphingomyelin (SM) or to the *cis* Golgi by means of membrane transport to be converted to glucosylceramide (GlcCer) by GlcCer synthase (GCS; Jeckel *et al*, 1992; Marks *et al*, 2001). Like Cer, GlcCer is produced on the cytosolic membrane leaflet (Jeckel *et al*, 1992; Marks *et al*, 2001). Here GlcCer is available for transport either by another lipid transfer protein, FAPP2, or, again, by membrane transport to the *trans* Golgi/TGN, where it is converted to lactosylceramide (LacCer) by LacCer synthase (*B4GALT5*, here referred as LCS; D'Angelo *et al*, 2007). LacCer is a branchpoint metabolite that feeds into the initiator enzymes of the GSL globo, ganglio, lacto and asialo GSL series that also localise at the *trans* Golgi/TGN (Merrill, 2011; D'Angelo *et al*, 2013b). To decipher the regulation of this finely compartmentalised metabolism, it is necessary to understand both the overall organisation of intra-Golgi transport (see below) and the molecular mechanisms that drive the localisation of individual GSL synthetic enzymes.

A broadly accepted model of intra-Golgi traffic is based on the mechanism of progression and maturation of the Golgi *cisternae* (schematised in Fig EV1B and C; Mironov *et al*, 1997; Bonfanti *et al*, 1998; Emr *et al*, 2009; Glick & Nakano, 2009; Nakano & Luini, 2010; Papanikou & Glick, 2014). In short, cargo-laden membranous carries leave the ER and reach the *cis* face of the Golgi stack, where they fuse to form new *cis cisternae*. At the same time, at the *trans* Golgi face "old" *trans cisternae* disassemble, to form anterograde carriers. This process generates a forward (*cis*-to-*trans*) flow of cisternal membranes (cisternal progression). The proteins destined for secretion (cargo proteins) remain in the progressing *cisternae* until they leave the Golgi *en route* to the PM or other destinations. The glycoenzymes behave differently. They also move forward within progressing *cisternae*, but, once reached their appropriate position in the stack, they flow backward via COPI coated vesicles. By doing so, they drive the compositional conversion or "maturation" of the *cis cisternae* into medial- and *trans* elements (Bonifacino & Glick, 2004; Rizzo *et al*, 2013; Willett *et al*, 2013; Jackson & Bouvet, 2014; Papanikou & Glick, 2014; Wong

& Munro, 2014; Ishii *et al*, 2016; Goud *et al*, 2018; Witkos *et al*, 2019). This happens in synchrony with cisternal progression. As a result, cargoes moving forward are successively exposed to the recycling enzymes present in each *cisterna*. The balance between the opposing anterograde and retrograde membrane fluxes regulates the sub-Golgi localisation of the GSL enzymes and hence the outcome of the competing GSL metabolic reactions (Fig EV1B and C).

Within the above framework, the specific molecular components that control the localisation of GSL metabolic enzymes remain unknown. We searched for interactions between GSL metabolic enzymes and the Golgi transport machinery. Most glycoenzymes are type II transmembrane proteins (Breton *et al*, 2006) with a luminal catalytic portion connected through a single transmembrane domain to a short N-terminal cytosolic tail (Breton *et al*, 2006). We found that many GSL enzymes contain, in their cytosolic tails, a motif that is present in yeast enzymes interacting with Vps74p (Tu *et al*, 2008). Vps74p is a membrane-associated protein that is recruited to the Golgi through its interaction with locally synthesised phosphatidylinositol-4-phosphate [PtdIns(4)*P*] (Wood *et al*, 2012). At the Golgi, Vps74p mediates the retro-transport of its client enzymes through the Golgi *cisternae* by sorting them into COPI vesicles (Schmitz *et al*, 2008; Tu *et al*, 2008; Wood *et al*, 2009; Liu *et al*, 2018; Casler *et al*, 2019). The mammalian homologue of Vps74p is GOLPH3. GOLPH3 rescues the localisation of glycoenzymes in the Vps74p null yeast mutant, indicating that it interacts with the Vps74p recognition motif in yeast enzymes and suggesting that it might bind to a similar motif in mammalian GSL synthetic enzymes (Tu *et al*, 2008; Eckert *et al*, 2014). Importantly, the *GOLPH3* gene is amplified in solid tumours, where it stimulates mitogenic signalling and cell proliferation, acting as an oncogene (Scott *et al*, 2009).

Following up on this lead, we found that GOLPH3 a) binds and sorts for intra-Golgi retro-transport a selected group of sequentially-acting GSL synthesising enzymes operating at the branchpoint among glycosphingolipid synthetic pathways (*i.e.* LCS, GM3 synthase [*ST3GAL5*, here referred as GM3S]; Gb3 synthase [*A4GALT*, here referred as Gb3S], and GD3 synthase [*ST8SIA1*, here referred as GD3S]) and b) exerts these effects by acting as an integral part of the cisternal maturation process (see above). Through these mechanisms, GOLPH3 operates as a master regulator of GSL metabolism, as it (i) determines the localisation of LCS and of other downstream-acting GSL enzymes in the *trans* Golgi *cisterna,* where they intercept the GlcCer conveyed to the *trans* Golgi by both vesicular and non-vesicular pathways (D'Angelo *et al*, 2007; D'Angelo *et al*, 2013b); (ii) regulates the levels of its client GSL enzymes by counteracting their transport to the lysosomes, where they are degraded; and (iii) regulates, through its client enzymes, the conversion of Cer (an onco-suppressor lipid) into growth-inducing GSLs of the globo and ganglio series. When expressed at high levels (*e.g.* in many cancer cells), GOLPH3 alters GSL metabolism promoting mitogenic signalling and cancer cell proliferation.

Results

GOLPH3 interacts with and retains in the Golgi selected GSL synthetic enzymes by binding their cytosolic tails

To identify links between GSL metabolism and intra-Golgi transport, we searched for physical and functional interactions between GSL

metabolic enzymes and the Golgi transport machinery. We found that 19 GSL enzymes accounting for 47.5% of the GSL synthetic pathway, bear a sequence in their cytosolic tail (*i.e.* L-x-x-[R/K], for brevity here referred to as LxxR) that is similar to the consensus sequence (F/L)-(L/I/V)-x-x-(R/K) in the tail of yeast enzymes reported to bind Vps74p (Tu *et al*, 2008). Other glycosylation enzymes do not show the LxxR sequence frequently, except the proteoglycan synthetic pathway, with 9 enzymes bearing this motif. These data, along with the finding that GOLPH3 rescues Vps74p null mutants (Tu *et al*, 2008), suggest that some enzymes of the GSL metabolic pathway interact with the mammalian Vps74p homologue GOLPH3. We will henceforth refer to Vps74p as Vps74p/GOLPH3.

We thus tested for binding between enzymes with key roles in GSL metabolism (see scheme in Fig EV1A) and GOLPH3, using biotinylated peptides corresponding to their cytosolic tails in co-precipitation and isothermal calorimetry experiments. We found that while Lc3 synthase (Lc3S) and galactosyltransferase 1 (GalT1), which are devoid of the LxxR motif, fail to interact with GOLPH3, all but one (GM2 synthase [B4GALNT1, here referred as GM2S]) of those that have LxxR (*i.e.* LCS, Gb3S, GM3S, and GD3S) show interaction (Figs 1A and EV1D). The known GOLPH3 interactor and LxxR-bearing enzyme C2GNT1 (Ali *et al*, 2012) served as positive control (Fig 1A).

We next examined whether the GOLPH3 binding causes retention of type II transmembrane proteins in the Golgi in living cells. We expressed a chimeric protein comprising GOLPH3-binding cytosolic tails (*i.e.* those of LCS, Gb3S, GM3S and GD3S) at the N-terminus of the transmembrane domain (TMD) of sucrose-isomaltase (SI), a type II integral PM protein, fused with GFP at the C-terminus ([enzyme]-SI-GFP); (Liu *et al*, 2018) in HeLa cells (in Appendix Table S11 are listed of cell lines used in this study). These reporters do not have Golgi retention signals in their TMD and luminal domains; thus, their retention can be ascribed only to the enzyme tails (Liu *et al*, 2018). As shown in Fig 1B, the GOLPH3-binding tails kept the reporter protein at the Golgi complex in a GOLPH3-dependent manner.

To characterise the GOLPH3 binding motif, we then focused on LCS, the best binder in the above co-precipitation assays that we also confirmed to co-immunoprecipitate GOLPH3 when expressed as a full-length protein in HeLa cells (Fig 1A and EV1E). We

introduced mutations in the LCS tail and tested the mutants for GOLPH3 binding (Fig 1C). Mutating either the LxxR-containing region or a positively charged amino acid cluster upstream of LxxR caused partial binding inhibition, indicating that, *in vitro*, GOLPH3 interacts with LCS tail through both regions. In *in vivo* Golgi retention experiments, however, mutations in the LxxR sequence markedly reduced Golgi localisation while mutations in the upstream positively charged residues had clearly milder effect, altogether indicating that LxxR is key for GOLPH3 recognition, reminiscent of the data in yeast (Fig 1D and E).

Finally, we sought functional evidence for a role of GOLPH3 in GSL metabolism. We overexpressed [OE (plasmids used in the study are listed in Appendix Table S9)] or silenced [knockdown, KD (siRNA sequences used in the study are listed in Appendix Table S1)] GOLPH3 in HeLa cells and used bacterial toxins in cytofluorimetric assays to reveal GSLs at the PM (Jacewicz *et al*, 1986; Russo *et al*, 2018). As shown in Fig 1F, we observed an increase in the levels of the globo series GSLs Gb3 [as assessed by Shiga toxin (ShTxB) (Jacewicz *et al*, 1986)] in GOLPH3 OE. On the contrary, GOLPH3 KD completely abolished both ShTxB and Cholera toxin (ChTxB; used as a marker of GM1 ganglioside; Gill & King, 1975; Russo *et al*, 2018) binding to HeLa cells. When other glycosylation pathways were assessed by lectin staining, we found that GOLPH3 OE induces a small increase in the level of sialylated glycans (see Additional Materials and Methods for experimental details) with no detectable effects on other major glycosylation pathways (Fig EV1F). Results coherent with these were also reported in a recent genome-wide CRISPR/Cas9 knockout (KO) screening in HeLa cells (Majumder *et al*, 2020), while N- and O-linked glycosylation pathways were found to be not significantly affected (Vladimir Lupashin personal communication).

In summary, a group of key GSL metabolic enzymes binds to GOLPH3 that retains them at the Golgi complex. Moreover, changes in GOLPH3 expression alter the levels of GSLs at the cell surface.

GOLPH3 determines the trans Golgi localisation of its clients across inter-converting cisternae

Glycosphingolipid synthetic enzymes downstream GlcCer synthesis are localised at the *trans* Golgi/TGN where they intercept both the

---

Figure 1. GOLPH3 interacts with the cytosolic tails of selected GSL synthetic enzymes.

A Pull-down experiments using as a bait the biotinylated peptides mimicking the N-terminal cytosolic tail of glycoenzymes performed from the whole HeLa cells lysates (top blot) or purified His-tagged GOLPH3 protein (bottom blot). The N-terminal cytosolic tail sequence of each glycoenzyme is indicated on the top of the blot (LxxR motif in red, biotin at the C-terminus). Immunoblotting shows affinity-captured GOLPH3 (endogenous and recombinant).

B Control or GOLPH3-KD HeLa cells expressing luminal SI-GFP or the chimeras of sucrose-isomaltase containing the N-terminal cytosolic tails of LCS, Gb3S, GM3S and GD3S were fixed and labelled for surface localised GFP (red). Scale bar, 20 μm.

C Pull-down experiments of biotinylated LCS WT and LCS mutant cytosolic tails from HeLa cells lysates (top blot) or purified His-tagged GOLPH3 protein (bottom blot). The N-terminal cytosolic tail of LCS WT and LCS mutants (mut. 1, 2 and 3) is shown on the top of the blot (mutations are in blue, LxxR motif in red, biotin is at the C-terminus).

D HeLa cells expressing luminal SI-GFP chimeras of sucrose-isomaltase (SI-GFP, green) containing the WT and mutant N-terminal cytosolic tails of LCS were fixed and labelled for surface localised GFP (red). Cells expressing LCS-SI-RxR and LCS-SI-LxxR chimeras show PM staining. Scale bar, 20 μm, (left). PM (surface) fluorescence intensity (in Appendix Table S10 are listed the software used in this study) of each chimera is normalised on the LCS-SI-GFP surface intensity (data are means ± SEM derived from two biological replicates; n is indicated in the graph, ***P < 0.001 [Student's t-test]) (right).

E Quantitative flow cytometry-based analysis of the experiment reported in (D); n is indicated in the graph (left). Percentage of cells with plasma membrane staining (surface) is reported for each chimera (right).

F GOLPH3-KD or OE HeLa cells were processed for ShTxB (upper panels) or ChTxB (lower panels) staining followed by flow cytometry analysis. Flow cytometry distributions and the relative scatter plots reporting the percentage of positive cells are shown for each condition.
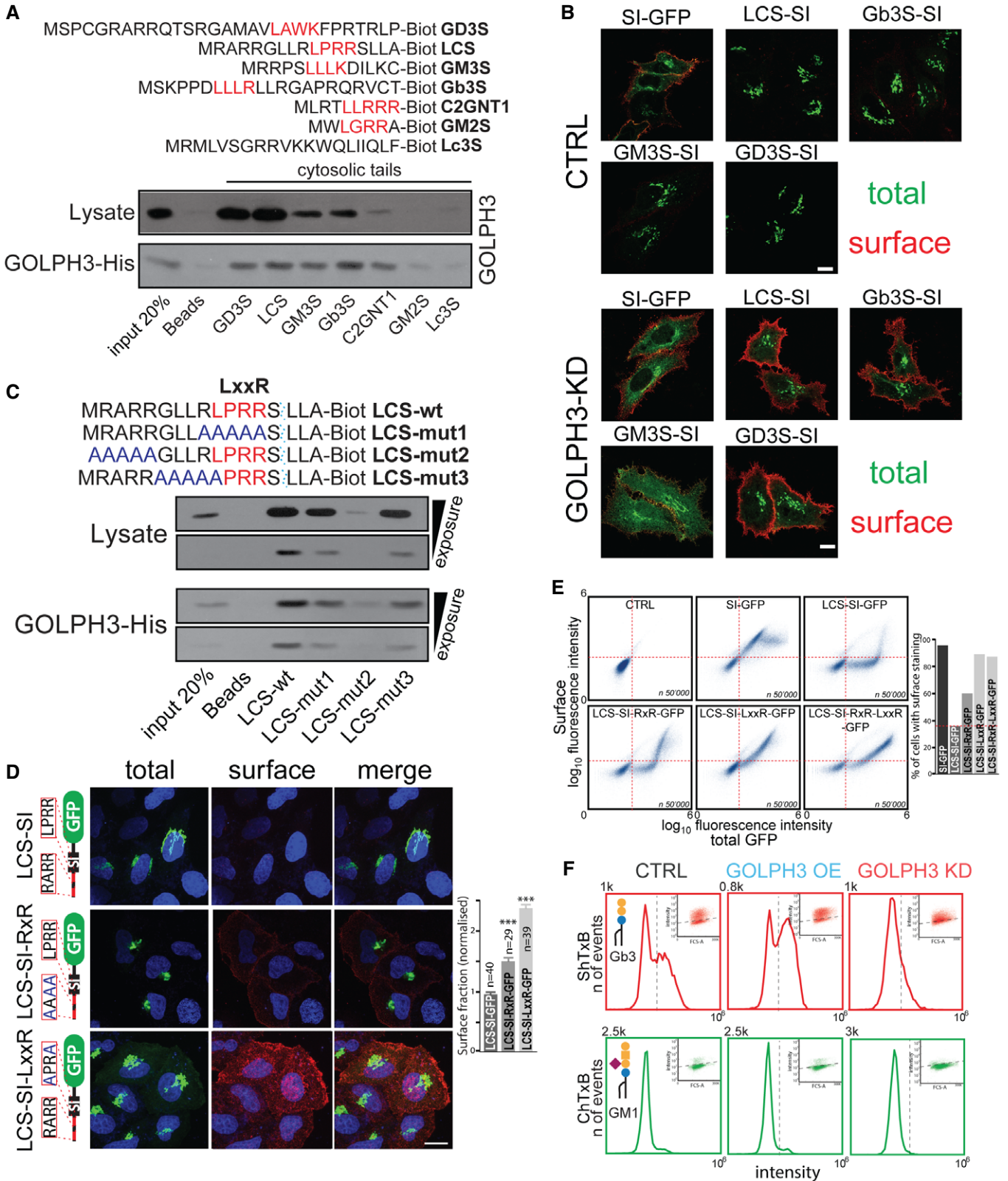
Source data are available online for this figure.

Figure 1.

vesicular and non-vesicular (*i.e.* FAPP2 mediated) fluxes of GlcCer to convert it into different complex GSLs (D'Angelo *et al*, 2013b). As shown above, the Golgi retention of these enzymes requires GOLPH3. GOLPH3 is recruited to the *trans* Golgi by a local pool of PtdIns(4)*P* generated by the PtdIns-4-kinase III beta (PI4KIIIB) (Dippold *et al*, 2009; De Matteis *et al*, 2013). Once recruited, GOLPH3 binds its client enzymes and incorporates them into COPI vesicles (Schmitz *et al*, 2008; Tu *et al*, 2008; Wood *et al*, 2009; Liu *et al*, 2018; Casler *et al*, 2019). This results in retrograde transfer of the enzymes through the secretory pathway (Tu *et al*, 2008). Given this background, what is the mechanism of localisation of the GOLPH3 clients in the *trans* Golgi *cisterna*?

To address this question, we examined whether GOLPH3 functions as part of the cisternal maturation mechanism, using LCS as a model client enzyme. We compared the transport of LCS and that of vesicular stomatitis virus G glycoprotein [VSV-G (all the viral vectors used in this study are listed in Appendix Table S6)], a traffic marker previously characterised to cross the Golgi by cisternal progression (Mironov *et al*, 2001) (see Materials and Methods for details). We first synchronised the Golgi transport of LCS using a LCS-GFP/KDEL-hook encoding plasmid [LCS-GFP_RUSH; LCS-GR for brevity; see Materials and Methods and Table S5 for a detailed description (Boncompain *et al*, 2012)] and monitored the transport of the LCS-GR in the presence or absence of GOLPH3. In control cells, LCS-GR, after leaving the ER, traversed the Golgi from *cis*-to-*trans* in < 20 min, and then remained in the *trans* Golgi, where LCS normally resides. Instead, in GOLPH3-KD cells, LCS-GR traversed the Golgi but was not retained in the *trans cisterna* and reached the TGN in less than 20 min (Fig 2A), from where it later moved to the lysosomes (see below).

Next, we co-expressed and co-synchronised LCS-GR and VSV-G and monitored their passage through the Golgi complex. In control cells, LCS-GR and VSV-G entered the Golgi and moved through the *cis* and medial Golgi compartments together. At this point, the two cargos segregated [*i.e.* VSV-G reached the TGN, while LCS-GR was retained in the *trans cisterna* (Fig 2B and C)]. In GOLPH3-KD cells,

instead, LCS-GR was not retained in the *trans* Golgi and reached the TGN together with VSV-G.

To gain further insight on the mode of LCS localisation, we used cryo-immunoelectron microscopy (cryo-IEM). Cryo-IEM showed that LCS-GR, during its progression from *cis*-to-*trans* Golgi (*i.e.* when it populates the *cis* and medial *cisternae*), is excluded from peri-Golgi vesicles. However, as LCS-GR reaches the *trans* Golgi (where it is retained), it enters the peri-Golgi vesicles (Fig 2D–F). In GOLPH3-KD cells, instead, LCS-GR never appears in peri-Golgi vesicles, it is not retained in the *trans cisterna* and crosses the stack up to the TGN in less than 20 min (Fig 2G and H). GalT1, a *trans* Golgi enzyme that does not bind GOLPH3 (see Fig EV1D and E), remained in the *trans cisterna* under both conditions, indicating the selectivity of action of GOLPH3 on the trafficking of its client LCS (Fig EV2A). These data suggest that GOLPH3 retains LCS in the *trans cisterna* by incorporating it into retrograde vesicles that carry it back towards proximal *cisternae*, hence preventing it from leaving the Golgi stack for the TGN. The simplest interpretation of these data is that LCS localises predominantly in the *trans cisterna* through recycling backward by GOLPH3 acting as a component of the cisternal maturation mechanism.

Cisternal maturation can be directly visualised in yeast (Losev *et al*, 2006; Matsuura-Tokita *et al*, 2006). We thus examined the mechanism of action of Vps74p (the GOLPH3 yeast homologue) on the trafficking of its client Mnn9p (Tu *et al*, 2008). At the steady state, Mnn9p populated the *cis* Golgi in wt cells (as all the Vps74p in yeast), while in Vps74p deprived (*vps74Δ*) cells, Mnn9p localised in the in the *trans* Golgi (as marked by Sys1p) and at the vacuole (Fig EV2B). Moreover, after 60 min of protein synthesis inhibition, Mnn9p was no longer in the Golgi in *vps74Δ* cells (Fig EV2C), while in wt cells it localised normally at the Golgi, indicating that, as for LCS and GOLPH3, the retention of Mnn9p at the Golgi depends on Vps74p. When Mnn9p transport was visualised by video microscopy *in vivo* (Pedelacq *et al*, 2006; Ishii *et al*, 2016), we observed that in wt cells Mnn9p was recycled out of the *cis cisterna* as soon

Figure 2. GOLPH3 drives the intra-Golgi recycling of LCS.

A   HeLa cells mock-treated or GOLPH3-KD were transiently transfected with LCS_GFP_RUSH (for simplicity, referred in the text as LCS-GR) and subjected to the synchronisation protocol described in Materials and Methods. Cells were then subjected to IF at each indicated time point: LCS-GR (green), *cis* Golgi marker GM130 (red) and TGN marker TGN46 (blue). Representative individual Golgi mini-stacks are shown. Scale bar, 1 μm. LCS-GR intra-Golgi trafficking in mock or GOLPH3-KD conditions it has been quantified (right graph) by computational coalescence of line scans, and was performed by normalised line scan analysis (normalisation of the distances was performed considering the GM130 peak as 0, and the TGN46 peak as 1). The n indicated in the graph refers to the number of Golgi stacks analysed in each condition.

B   Mock and GOLPH3-KD HeLa cells co-expressing LCS-GR and VSV-G were subjected to the co-synchronisation protocol described in Materials and Methods. Cells were then subjected to IF: LCS-GR or VSV-G (green), GM130 (blue) and TGN46 (red). Representative individual Golgi mini-stacks are shown. Scale bar, 1 μm.

C   Quantification of the experiment in (B) was performed by normalised line scan analysis (normalisation of the distances was performed considering the GM130 peak as 0, and the TGN46 peak as 1); n indicated in the graph refers to the number of Golgi stacks analysed in each condition, individual data points and means $\pm$ SEM are shown, ***$P < 0.001$ (Student's *t*-test); ns, not significant.

D   HeLa cells were transfected with LCS-GR, subjected to the synchronisation protocol (see Materials and Methods), fixed and processed for cryoimmunolabeling with an anti-GFP antibody (15 nm gold particles) and anti-GM130 antibody (10 nm gold particles, black arrowheads) peri-Golgi vesicles containing LCS-GR are marked by red arrowheads. Scale bar, 150 nm.

E, F   Quantification of the distribution of LCS-GR as measured by frequency distribution analysis (E) and linear density (LD, in (F)) (data are means $\pm$ SEM, number of Golgi stacks is $n = 15$ at 0 min, $n = 14$ at 10 min, $n = 17$ at 20 min. (E) The red arrows indicate the fraction of LCS-GR gold particles (%) in vesicles at each indicated time point.

G   HeLa cells expressing LCS-GR mock or GOLPH3-KD were treated and stained as in (D). Black arrowheads indicate GM130; peri-Golgi vesicles containing LCS-GR are marked by red arrowheads. LCS-GR in the TGN is marked by blue arrowheads. Scale bar, 150 nm.

H   Quantification of LCS-GR distribution (linear density, LD) across the stack and in peri-Golgi vesicles (data are means $\pm$ SEM, number of Golgi stacks is $n = 17$ at 20 min for the CTRL, $n = 13$ at 20 min for the GOLPH3 KD; *$P < 0.05$, **$P < 0.01$; ***$P < 0.001$ [Student's *t*-test]).
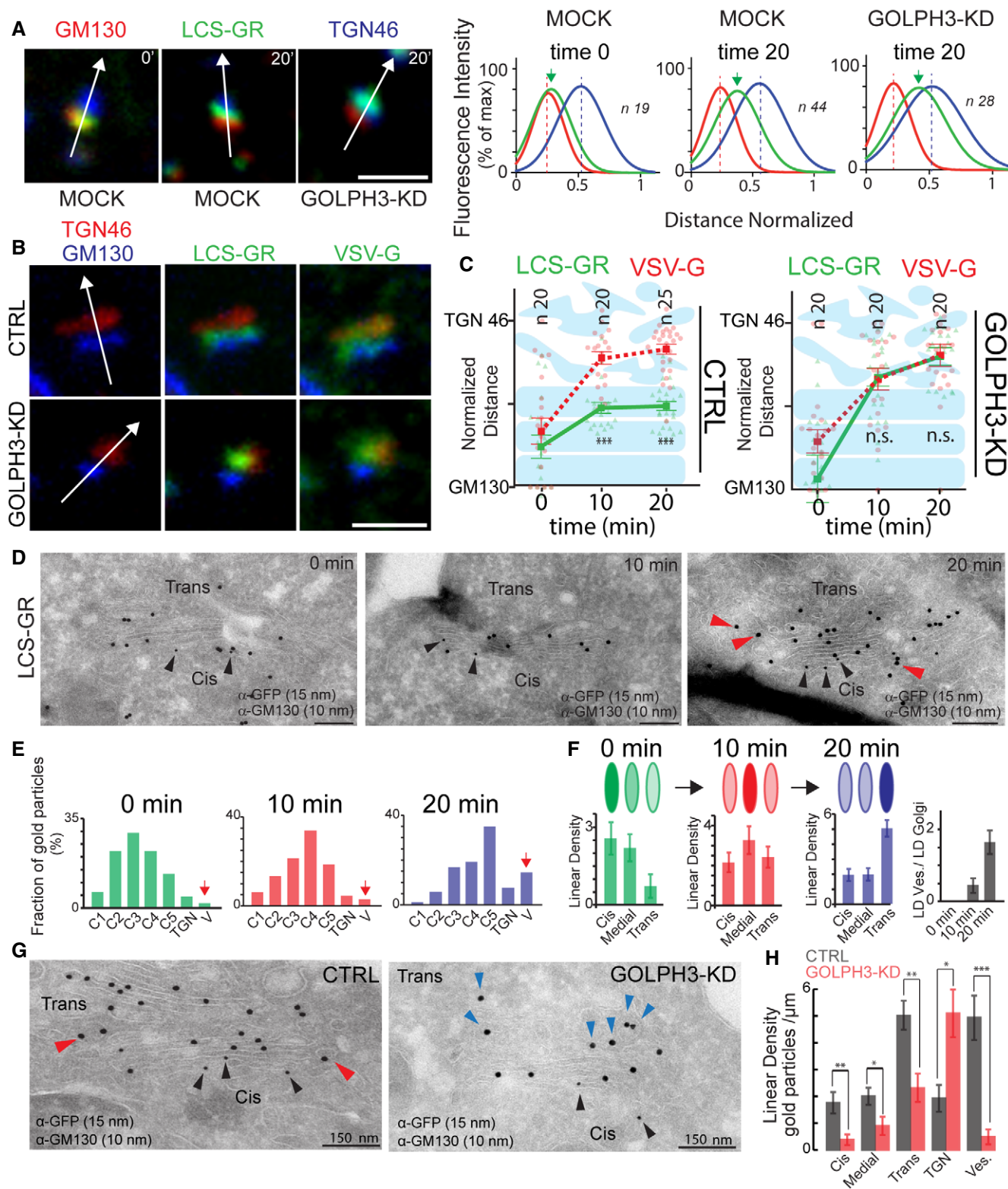
Figure 2.

as this *cisterna* started converting into a *trans* element (as monitored by the acquisition of the *trans* marker Sys1p) (Losev *et al*, 2006; Matsuura-Tokita *et al*, 2006; Pedelacq *et al*, 2006). On the contrary, in *vps74Δ* cells Mnn9p remained in the *cisterna* longer, until it was filled with the Sys1p *trans* marker (Fig EV2D), and then left it, to possibly move to the vacuole.

To test this possibility, we "visually" synchronised the movement of Mnn9p through the secretory pathway using the superfolder-GFP tag (Mnn9p-sfGFP; Pedelacq *et al*, 2006). We photobleached Mnn9p-sfGFP and monitored the newly synthesised Mnn9p-sfGFP as it progressed through the secretory pathway. In wt cells, newly synthesised Mnn9p-sfGFP was quickly transported (2-4 min) to the Golgi and then remained there for the duration of the experiment (*i.e.* up to 30 min), while in *vps74Δ* cells Mnn9p-sfGFP was not retained and proceeded to the vacuole within 5 min (Fig EV2E). Notably, these differences in traffic are not due to variations in the Mnn9p-sfGFP synthetic rates between the two yeast strains (Fig EV2F), and the transport rate of Mnn9p-sfGFP to the vacuole in *Vps74Δ* cells is similar to that of a vacuolar cargo protein (Vph1p-sfGFP) (Fig EV2G). These results demonstrate that Vps74p/GOLPH3 acts as a component of the cisternal inter-conversion mechanism also in yeast.

GOLPH3 regulates the levels of its client enzymes by counteracting their transport to the lysosomes and hence their degradation

Prompted by the effects of Vps74p/GOLPH3 on the intra-Golgi trafficking of their clients, we examined how GOLPH3 impacts the GSL enzymes under steady-state conditions. The results were unexpected. GOLPH3 OE increased the levels of endogenous LCS at the Golgi both in primary human fibroblasts (PHFs) and in HeLa cells (Fig 3A and B), as judged by immunofluorescence (IF), while GOLPH3 KD had the opposite effect, in PHFs (Fig 3A). In HeLa cells, the consequence of GOLPH3 KD on endogenous LCS was difficult to assess because of the very low expression levels of this enzyme. We thus performed similar experiments using HA-tagged LCS. We found that in HeLa cells GOLPH3 KD (and OE) had effects similar to those observed in PHFs on endogenous LCS. In addition, GOLPH3 OE partially redistributed LCS to the ER (Fig 3C), reminiscent of analogous observations in yeast (Tu *et al*, 2008). Western blot experiments confirmed that GOLPH3 OE increased, and GOLPH3 KD decreased, the LCS-HA protein levels in HeLa cells, in agreement with the IF data (Fig EV3D).

Cryo-IEM showed that, in control cells, LCS-HA is concentrated at the *trans* Golgi, as expected, with lower levels in the TGN and in medial and *cis cisternae*, and is detectable in peri-Golgi vesicles, some of which are also decorated by GOLPH3 (Fig EV2H and I). GOLPH3 OE caused a moderate shift of LCS from *trans* towards early Golgi compartments and increased the LCS-HA density in peri-Golgi vesicles. On the contrary, GOLPH3 KD resulted in low LCS-HA levels in the Golgi stack and in the absence of LCS-HA from vesicles (Fig EV2H).

The changes in levels of LCS induced by GOLPH3 OE could be either due to changes in LCS synthesis or in LCS degradation. The data with the LCS-HA construct, which is expressed under a constitutive promoter, point against a GOLPH3 effect on LCS transcription; moreover, we found no differences in the endogenous LCS (encoded by *B4GALT5*) mRNA levels between GOLPH3 OE or KD cells (Fig EV2J) (see Table S8 for the list of commercial assays and kits used in this study). This indicates that GOLPH3 does not affect LCS transcription and that it might regulate LCS degradation.

To test this possibility, we monitored the trafficking of LCS through the secretory pathway using LCS-GR and video microscopy. Neither GOLPH3 KD nor GOLPH3 OE influenced the transport of LCS-GR from the ER to the Golgi (Fig 3D and E and Movie EV1). Instead, the exit of LCS-GR out of the Golgi was markedly affected. In control cells, LCS-GR persisted in the Golgi region for ~4 h before dissipating into punctate cytosolic structures that could be counterstained with the lysosomal marker LAMP1 (Fig EV3A) and then disappeared; in GOLPH3 KD cells, LCS-GR entered the LAMP1-positive structures much more rapidly, within about 2 h (with most of this time being spent in the transport between ER and Golgi and through the TGN to the lysosomes); and in GOLPH3-OE cells, LCS-GR remained at the Golgi for up to 10 h (longest recording time) and never made it to LAMP1-positive *puncta* (Figs 3D and EV3A and Movie EV1).

These results indicate that GOLPH3 KD decreases the Golgi retention of LCS and allows LCS to reach the lysosomes, where it is degraded. GOLPH3 OE, instead, enhances the Golgi retention and residence time of LCS, impeding its arrival at the lysosomes. Control cells show an intermediate phenotype: A fraction of LCS constantly

---

Figure 3. GOLPH3 regulates the lysosomal degradation of its clients.

A PHFs GOLPH3 OE (left), or KD (right), were fixed and processed for IF: Endogenous LCS (green), GOLPH3 (red), TGN46 or DAPI (blue). Dashed lines indicate cells overexpressing or interfered for GOLPH3. Scale bar, 20 μm. Quantification of the amount of endogenous LCS (right graph) at the Golgi; data are means ± SEM derived from two biological replicates, $n = 42$ in CTRL, $n = 49$ in GOLPH3 KD and $n = 27$ in GOLPH3 OE; ***$P < 0.001$ [Student's *t*-test]).

B GOLPH3-OE HeLa cells were fixed and processed for IF: Endogenous LCS (green), GOLPH3 (red) and TGN46 (blue). Dashed lines indicate cells overexpressing GOLPH3. Scale bar, 20 μm. Quantification of the amount of endogenous LCS (right graph) at the Golgi (data are means ± SEM derived from two biological replicates, $n = 21$ in CTRL, $n = 11$ in GOLPH3 OE; ***$P < 0.001$ [Student's *t*-test]).

C GOLPH3 OE or KD HeLa cells expressing LCS-HA were fixed and processed for IF: HA (green). Asterisks indicate GOLPH3 OE cells. Scale bar, 20 μm.

D Assessment of LCS-GR synchronised transport in GOLPH3 OE or KD HeLa cells. Micrographs show cells at the indicated trafficking time points. Scale bar, 20 μm.

E Representative WB of cells treated as in (D) ($n = 3$).

F Plots of the densitometric quantification of the amount of LCS-GR (Golgi mature band) over time, starting from 2 h chase (data are means of at least 3 experiments ± SD).

G GOLPH3 OE or KD HeLa cells expressing LCS-HA were treated with bafilomycin A1 (BafA1, 10 nM) for 16 h, fixed and processed for IF labelling: LCS (green), LAMP1 (red) and DAPI (blue). Arrowheads indicate LCS and LAMP1 co-localisation. Scale bar, 20 μm.

H WB of cells treated as in (G). Densitometric quantification of the blot is plotted in the top panel (data are means of at least 3 experiments ± SD).

I GOLPH3 OE or KD HeLa cells expressing the indicated HA-tagged glycoenzymes were fixed and processed for IF. Asterisks indicate GOLPH3 OE cells. Scale bar, 20 μm.

J Number of glycoenzymes-HA-positive spots per cell in GOLPH3-KD cells (left panel) and percentage of cells with glycoenzymes-HA in the ER in GOLPH3-OE cells (right panel) are plotted (n is indicated in the graph; data are means ± SEM; ***$P < 0.001$ [Student's *t*-test]).

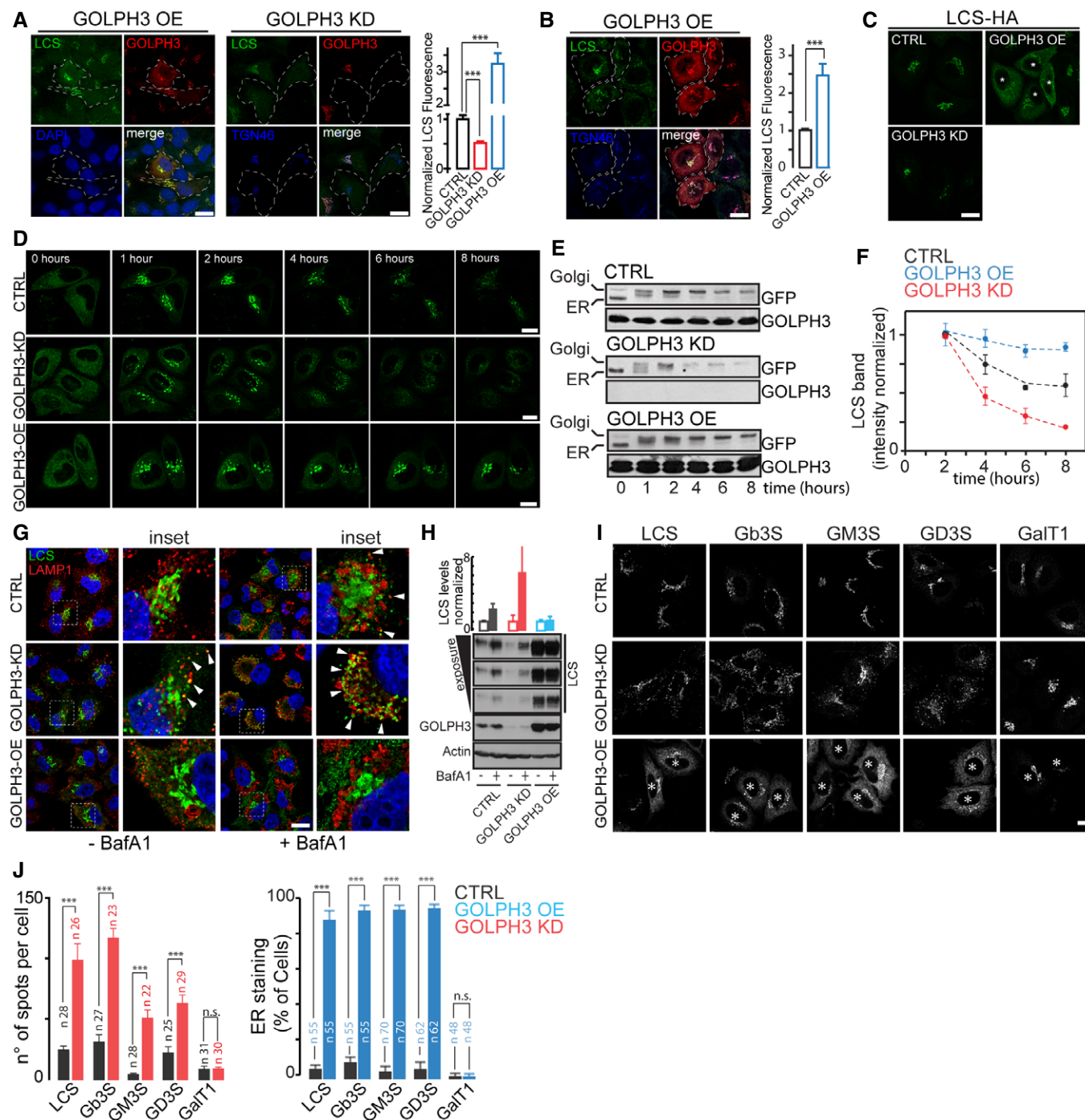Source data are available online for this figure.

Figure 3.

escapes the Golgi and reaches the lysosomes, resulting in a relatively fast basal degradation rate of this enzyme.

We next evaluated by Western blotting the LCS-GR protein levels during synchronised transport. In control cells, the LCS-GR protein levels started to decline after acquiring full glycosylation features, *i.e.* after arrival at the Golgi, with a half-time of ~4 h. In GOLPH3-KD cells this decline was faster (half-life ~1–2 h), while in GOLPH3-OE cells the decline was extremely slow, or not detectable for up to 8 h after release from the ER (longest time

point tested Fig 3E and F). Control experiments with GalT1 (not a GOLPH3 client) in its GFP_RUSH form showed that this enzyme is not affected by GOLPH3 OE or KD (Fig EV3B). Thus, LCS is retained in the Golgi with an efficiency that depends on the levels of GOLPH3; and once it escapes the GOLPH3-dependent retention mechanisms, it reaches the lysosomes and is degraded (Figs 3D and EV3A).

To test these conclusions, GOLPH3 OE and KD experiments were conducted in the presence of the lysosomal degradation inhibitor

bafilomycin (Yoshimori *et al*, 1991; in Appendix Table S7 are listed all the chemicals used in this study). As shown in Fig 3G and H, inhibition of lysosomal degradation caused accumulation of LCS protein (specifically in LAMP1-positive compartment) that was detectable in control conditions, noticeably marked in GOLPH3 KD and not visible in GOLPH3 OE.

We then examined the impact of GOLPH3 on its other client enzymes, *e.g.* Gb3S, GM3S and GD3S, again using HA-tagged constructs due to lack of suitable antibodies. The impact of GOLPH3 on the cellular localisation and protein levels of these enzymes was very similar to that observed on LCS (Figs 3I and J and EV3C and D). In contrast, numerous other *trans* Golgi located enzymes that do not bear the LxxR GOLPH3 recognition motif in their cytosolic tails and/or are not GOLPH3 clients (*i.e.* GalT1; sphingomyelin synthase 1 [SMS1]; glucosylceramide synthase [here referred as GCS]; B3GNT5 [here referred as Lc3S]; GM2S and GM1 synthase [B3GALT4, here referred as GM1S]) were insensitive to manipulations of GOLPH3 levels (Figs 3I and J and EV3D and E). The effects of GOLPH3 on tagged expressed enzymes reflect those on the endogenous ones, as indicated by two lines of evidence: (i) the consequences of GOLPH3 manipulation on endogenous and HA-tagged are very similar in the case of LCS, for which this comparison is possible; (ii) the impact of GOLPH3 on GSL metabolism is coherent with the observed effects of GOLPH3 on its exogenously expressed clients (as shown below).

Next, as a form of precaution, we considered that GOLPH3 might have an additional mechanism of action. GOLPH3 is a known regulator of mTORC1 signalling (Scott *et al*, 2009). As mTORC1 suppresses lysosomal biogenesis and promotes protein synthesis (Shimobayashi & Hall, 2014), a possible interpretation for the observed phenotypes would be that GOLPH3 controls the levels of GSL enzyme through mTORC1. To test this hypothesis, cells overexpressing GOLPH3 were treated with the mTOR inhibitor Torin and the levels of LCS-HA were considered. As shown in Fig EV3F, GOLPH3 OE increased LCS-HA levels irrespective of mTOR activation.

These collective data suggest that GOLPH3 regulates the levels of its clients by driving their retro-transport from the *trans cisterna*, thereby enhancing their Golgi retention and preventing their escape to the lysosomes and consequent degradation. This model implies that competing for GOLPH3 binding should impair Golgi retention of GOLPH3 clients. To directly test this prediction, we overexpressed SI-GFP chimeras bearing GOLPH3-binding cytosolic tails and looked at the effect of the overexpression on the localisation of LCS-HA. As shown in Fig EV3G overexpression of all the 4 chimeras bearing GOLPH3-binding cytosolic tails (*i.e.* LCS-SI, Gb3S-SI, GM3S-SI and GD3S-SI) induced LCS-HA redistribution to cytosolic *puncta* while the overexpression of the SI-GFP chimera bearing the non-GOLPH3-binding cytosolic tail of GalT1 did not.

In all, when GOLPH3 binding to its clients is compromised (i.e. in GOLPH3 KD of by competing with GOLPH3 binding site), the client enzymes escape to the lysosomes, and their levels decrease. In control cells, GOLPH3-dependent retention is suboptimal and allows a fraction of the clients to reach the lysosomes, resulting in a constitutively fast degradation (with a half-time of ~4 h) of these enzymes. This is crucial as it makes the client enzymes amenable to regulation by GOLPH3. Thus, GOLPH3 OE (a condition found in

several tumours) inhibits lysosomal degradation and hence increases their levels (Fig EV3D and H).

GOLPH3 reprograms the GSL metabolism through its client GSL enzymes

Do the GOLPH3-induced changes on its GSL client enzymes have metabolic consequences? The enzymes controlled by GOLPH3 represent a key metabolic hub in GSL biosynthesis. Indeed, the LCS → Gb3S and LCS → GM3S → GD3S axes convert the common precursors LacCer into the globo and ganglio GSL series, respectively, at the expense of GlcCer and Cer. GOLPH3, therefore, controls specific GSL enzymes and does not impact all the GSL pathways. Its manipulations are thus expected to alter the GSL metabolic pattern. We evaluated the impact of GOLPH3 on the GSL metabolism both in HeLa cells and PHFs.

We first examined the GSL synthetic flux by [^{3}H]-sphingosine pulse and chase experiments (see Materials and Methods for details) in both HeLa cells and PHFs (Figs 4A and EV4A). GOLPH3 KD decreased the production of the metabolite pool downstream of LCS (with marked effects on Gb3 and GM3) and caused the accumulation of the metabolites upstream LCS (*i.e.* of GlcCer and, moderately, of Cer). On the opposite, GOLPH3 OE enhanced the production of the metabolites downstream LCS (specifically of Gb3) and accelerated the turnover of the metabolites upstream this enzyme. The disparity of the GOLPH3 OE effect on Gb3 and GM3 (strong on the former and nearly absent on the latter) is likely to be due to the prevalence of the activity of Gb3S over that of GM3S in HeLa, as these enzymes compete for the same substrate (*i.e.* LacCer). The enhanced substrate consumption by Gb3S for Gb3 production might therefore have flattened the expected GM3 increase.

Steady-state mass spectrometry and toxin-based cytofluorometry measurements were broadly in agreement with the pulse and chase data. GOLPH3 KD induced a decrease in the metabolites downstream LCS and an increase in those upstream it, and GOLPH3 OE had the opposite effects (Figs 4B–D and EV4B; also compare with Fig 1F). Interestingly, GOLPH3 OE decreased the strong growth-arrest inducer C16:0 Cer (Kroesen *et al*, 2001; Fekry *et al*, 2018) both in HeLa cells and PHFs (Fig 4E). Importantly, the untargeted lipidomics of GOLPH3-KD and GOLPH3-OE HeLa cells did not show significant changes in other segments of the lipid metabolism (Fig EV4C). GOLPH3 had similar metabolic impact in HeLa cells and PHFs with minor differences (Figs 4A and B and EV4A and B) that can be explained by the different expression levels of LCS and Gb3S in the two lines.

Finally, given the pivotal position of the GOLPH3 client LCS in the GSL pathway, we examined whether changes in LCS levels mimic those of GOLPH3 on GSL metabolism. As shown in Figs 4B and E, and EV4B and D, LCS OE increased the levels of both LacCer and Gb3, although with a stronger effect on LacCer, as expected, and reduced Cer, while LCS KD had the opposite effects. The consequences of LCS manipulations thus recapitulate those induced by GOLPH3 in parallel experiments. Moreover, the depletion of LCS inhibited the effects of GOLPH3 on GSLs production and specifically on Gb3 (Fig EV4E). Thus, LCS mimics GOLPH3 and is required for the GOLPH3 effects on GSL metabolism.
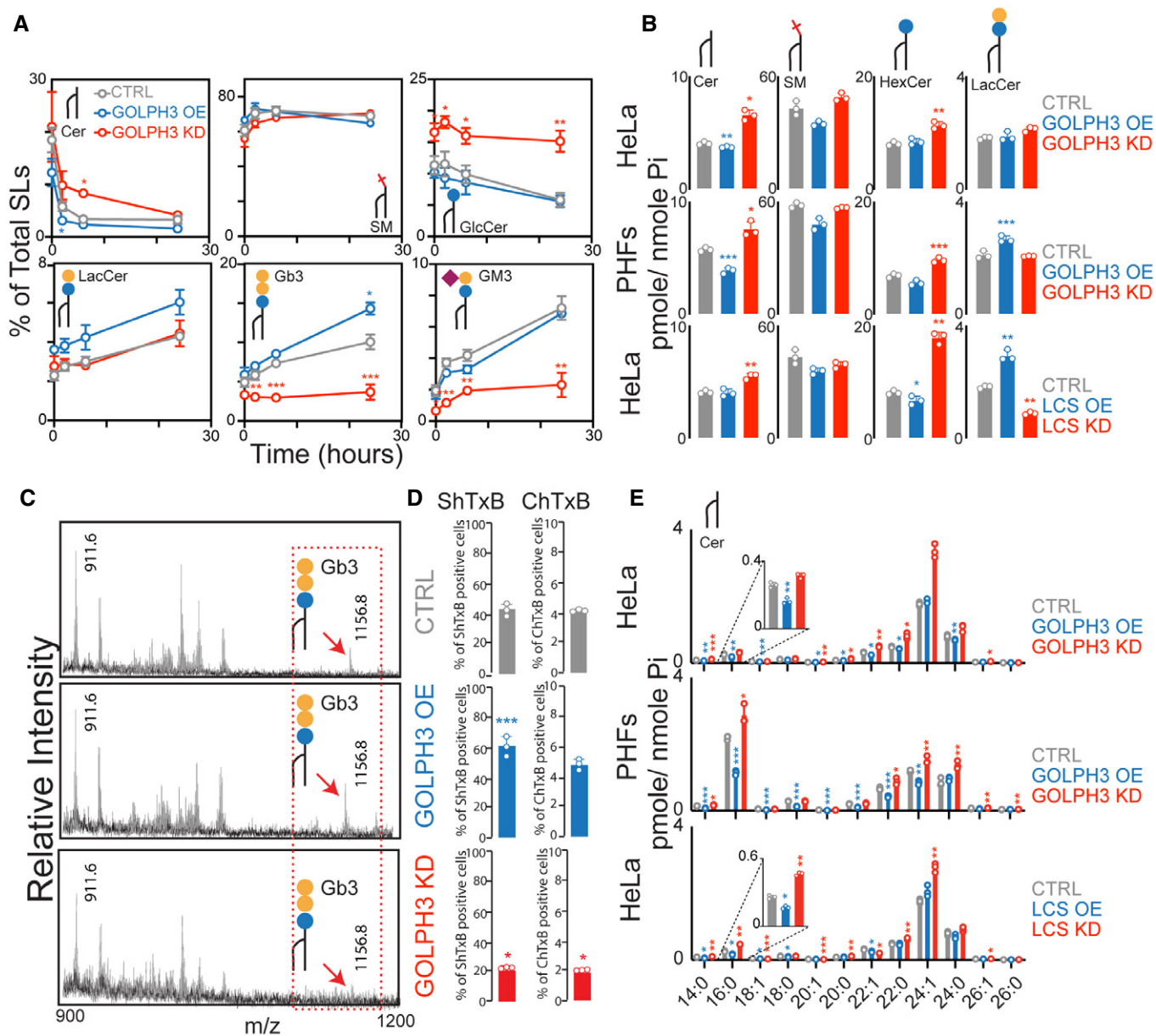
Figure 4. GOLPH3 controls GSL synthesis.

A Effects of GOLPH3 KD or OE on glycosphingolipid synthetic flux as assessed by [³H]-sphingosine pulse (2 h) and chase (indicated times), lipid extraction and HPTLC separation and radioactive counting (data are means ± SD of at least three independent experiments; *P < 0.05, **P < 0.01, ***P < 0.001 [Student's t-test]).

B Effects of GOLPH3 KD or OE on sphingolipid levels as assessed by LC/MS of HeLa cells (top) and PHFs (middle). Effects of LCS KD or OE on sphingolipid levels as assessed by LC/MS of HeLa cells (bottom) (data are means ± SD of at least three independent experiments; *P < 0.05, **P < 0.01, ***P < 0.001 [Student's t-test]). Targeted lipidomics data from this study are available at Metabolomics Workbench database with the following IDs: ST001673 for HeLa cells, and ST001672 for PHFs.

C Effects of GOLPH3 KD or OE on Gb3 as assessed by MALDI-MS after lipid extraction. Profiles are representative of 3 independent experiments. Untargeted lipidomics data from this study are available at Metabolomics Workbench database with the following ID: ST001674.

D Histograms reporting the percentage of ShtxB or ChTxB-positive cells in each condition as in Fig 1F (data are means ± SD of at least three independent experiments; *P < 0.05, ***P < 0.001 [Student's t-test]).

E Effects of GOLPH3 KD or OE on ceramide levels as assessed by LC/MS of HeLa cells (top) and PHFs (middle). Effects of LCS KD or OE on ceramide levels as assessed by LC/MS of HeLa cells (bottom). The dotted black box highlights the effects on C16:0 Cer (data are means ± SD of at least 3 independent experiments; *P < 0.05, **P < 0.01, ***P < 0.001 [Student's t-test]). Targeted lipidomics data from this study are available at Metabolomics Workbench database with the following IDs: ST001673 for HeLa cells, and ST001672 for PHFs.

Altogether, the effects of GOLPH3 (and of LCS) on GSL metabolism are coherent with those of GOLPH3 on GSL metabolic enzymes, as shown in the scheme in Fig EV4F.

GOLPH3-induced cell proliferation requires its client GSL metabolic enzymes

The GOLPH3 gene is amplified in many tumours where GOLPH3 exerts oncogenic properties (Scott et al, 2009). Are the effects of GOLPH3 on GSL metabolism involved in the GOLPH3-induced cancer cell proliferation? The overexpression of GOLPH3 activates mitogenic pathways (Scott et al, 2009; Scott & Chin, 2010; Zeng et al, 2012), including the PI3K, Akt, mTOR and p21^{waf} cascade and induces cell growth (Scott et al, 2009; Zeng et al, 2012). GSLs that are increased by GOLPH3 OE have also been reported to activate growth factor receptors and integrin signalling (Hakomori Si, 2002; Steelant et al, 2002; Park et al, 2012; Chuang et al, 2019; Furukawa et al, 2019). We thus examined whether the mitogenic properties of GOLPH3 are mediated by GSL metabolic changes.

We first verified that, as reported for other cell systems, in HeLa cells GOLPH3 OE induces cell proliferation in an mTOR dependent manner (Fig EV4G). Then, we compared the impact of LCS OE or KD with that of GOLPH3 on these signalling pathways and on proliferation. Remarkably, LCS OE in HeLa cells and PHFs mimicked the stimulatory effects of GOLPH3 OE on Akt and mTOR signalling (i.e. it increased phosphorylation of Akt [at Thr308 and Ser473], and of both p70S6k and 4E-BP1), as well as on the expression of p21^{waf}. Conversely, the depletion of LCS had consequences similar to those of GOLPH3 KD, i.e. depressed the basal activity of the Akt-mTOR pathway and enhanced the expression of p21^{waf} (Figs 5A, and EV4H). LCS phenocopied GOLPH3 also in assays of cell proliferation as judged by growth in adherence and in soft agar (Fig 5B and C).

We also asked whether synthesis of GSLs is necessary for GOLPH3-induced mitogenesis. To this end, we examined the effects of GOLPH3 OE in LCS KD as well as in GCS-KO and LCS-KO HeLa cells (Yamaji & Hanada, 2014). As expected, in both GCS-KO and LCS-KO cells the production of complex GSLs was strongly inhibited (Fig EV4I). Under these conditions (and in LCS KD HeLa cells), GOLPH3 OE was unable to induce activation of Akt/mTOR signalling and to stimulate anchorage-independent growth (Fig 5A, C–E). Overexpressing LCS re-established GSLs production (Fig EV4I) and promoted growth in LCS-KO cells; however, it had no effect in GCS-KO cells, indicating that, as expected, LCS requires the presence of the upstream metabolite GlcCer to induce growth, and so ruling out spurious effects of LCS through reactions on GSL-unrelated substrates. Notably, LCS-KO cells could be induced to grow also by the expression of an unrelated oncogene i.e. RAS-Val12 (Sweet et al, 1984) (Fig EV4J), indicating that LCS is required for GOLPH3 dependent growth, but not for growth in general.

We further asked whether the LCS product LacCer needs to be converted into Gb3 to activate mitogenic signalling. To test this possibility, we depleted Gb3S and monitored the signalling response to GOLPH3 OE. As shown in Fig EV4K and L, depletion of Gb3S inhibited the mitogenic signalling and anchorage-independent growth induced by GOLPH3 OE. Thus, the GCS-LCS-Gb3S GSL metabolic axis that leads to Gb3 production is needed for the GOLPH3-induced mitogenesis in our model cells. In sum, the enhancement of the GCS-LCS-Gb3S GSL metabolic axis is responsible, at least in

part, for the GOLPH3 mitogenic and oncogenic effects; in addition, the decrease of the onco-suppressor Cer that accompanies these changes is likely to contribute to the stimulation of cell growth.

We finally asked whether the GSL-dependent mechanism of action of GOLPH3 in cell proliferation applies to cancer cell lines exhibiting GOLPH3 amplification. To test this, we first examined two prostatic cancer cell lines, LNCaP and DU145, of which the latter shows GOLPH3 genomic amplification [according to the cBioPortal database; http://www.cbioportal.org/; (Gao et al, 2013)]. This line showed higher levels of both GOLPH3 and LCS as well as of complex GSLs (among which Gb3) compared to LNCaP cells (Fig EV4M and N). Moreover, the DU145 line displayed stronger basal phosphorylation of the mTOR substrates p70S6k and p4E-BP1 than LNCaP cells (Fig EV4M), all features consistent with the genomic amplification and the higher GOLPH3 levels. When we depleted LCS (or GOLPH3) in either the DU145 or in the LNCaP cell lines (Fig EV4N), the growth of the DU145 cells was potently inhibited, while LNCaP cells were much less affected, as judged by the soft agar colony formation assays (Fig 5F). Thus, GOLPH3 amplification and GOLPH3 overexpression correlate with increased LCS protein levels and with the requirement for LCS for growth, in line with the above results obtained in HeLa cells. Altogether, these experiments indicate that GOLPH3 induced mitogenic signalling and cell growth require the increased expression of its client enzymes, and production of LacCer and Gb3 (and possibly of downstream globosides).

LCS and GOLPH3 levels correlate in human cancers

The above data indicate that GOLPH3 increases LCS levels to induce proliferation in experimental cells. We reasoned that, if the mechanism identified in this study operates in human cancer, a correlation should be detectable between GOLPH3 and LCS protein levels also in cancer tissue from patients. The GOLPH3 gene has been originally reported to be amplified in different tumour types, with a particularly high frequency (56%) in non-small cell lung cancer (NSCLC) (Scott et al, 2009), and our database search for GOLPH3 copy number variations/alterations (CNVs) in large cohorts of lung cancer patients (when using stringent defining criteria) returns significant, though lower, amplification frequencies (~10%) [cBioPortal; http://www.cbioportal.org/; (Gao et al, 2013)] (Fig EV4O and P). Also, the GOLPH3 protein levels have been reported by many studies to be higher in cancer than in healthy lung tissue in > 70% of tumour biopsies from NSCLC patients and to correlate with poor survival (Tang et al, 2016; Tang et al, 2018). Using a tissue microarray (TMA) prepared from a limited number (n = 72) of surgical specimens from NSCLC patients (22 females and 50 males with median age at surgery of 63.5 years) (Fig 6A), we examined the correlation between the levels of GOLPH3 and those of LCS. We analysed GOLPH3 CNVs by fluorescence in situ hybridisation (FISH) (Fig 6B) and GOLPH3 and LCS protein levels by immunohistochemistry (IHC) (Fig 6C and D). As shown in Fig 6B and C and in Table EV1, ~12% and ~40% of the analysed samples had a GOLPH3 CN > 6 (amplification) and > 4 (gain), respectively, and > 60% of the analysed samples displayed clearly measurable GOLPH3 protein expression levels, in line with previous reports (Tang et al, 2016; Tang et al, 2018). When we examined the LCS protein, we found that cancer samples with high GOLPH3
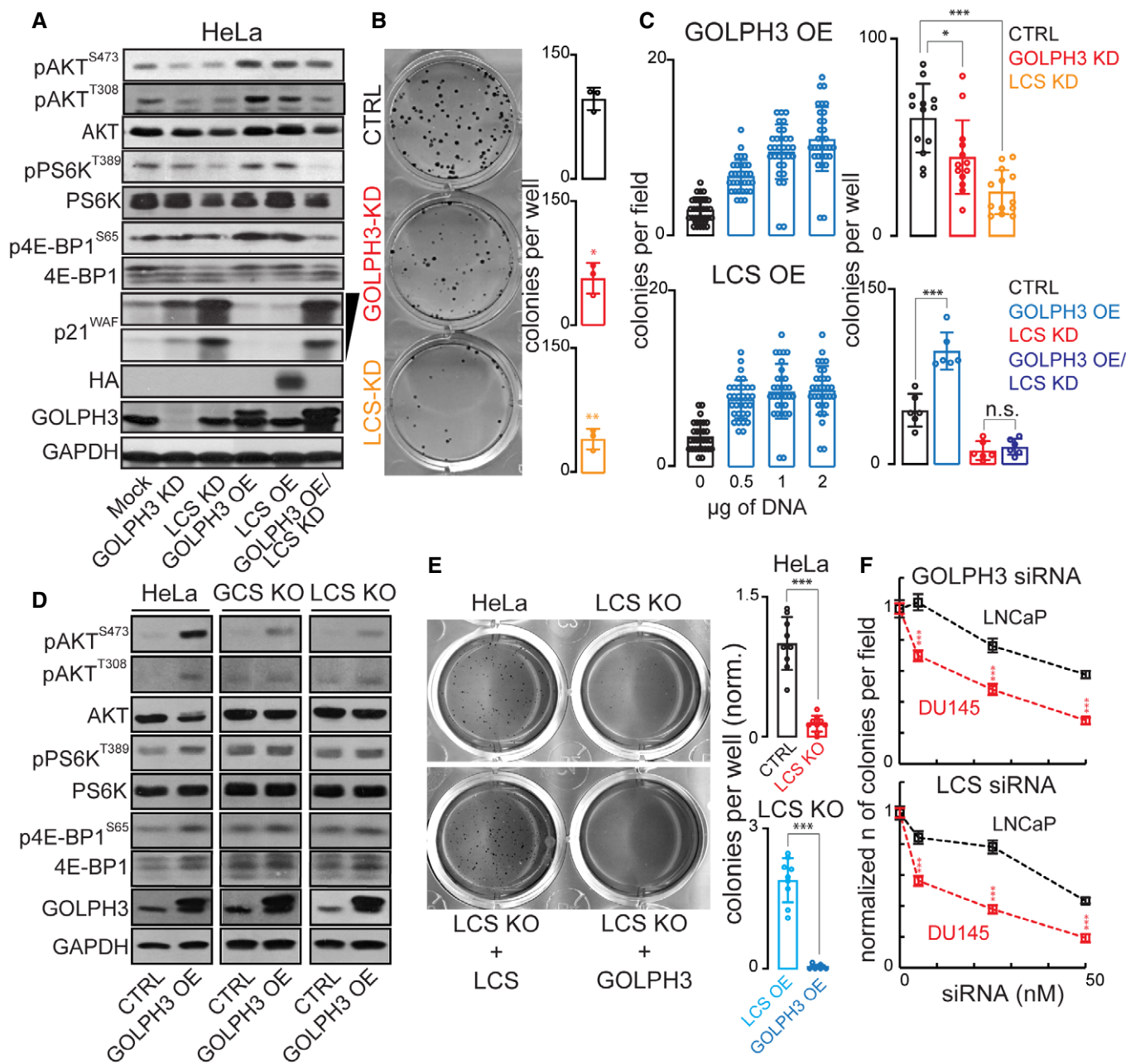
Figure 5. GOLPH3 impacts growth signalling through LCS.

A   Cell lysates from HeLa cells KD or OE for either GOLPH3 or LCS were processed for SDS–PAGE and Western blotting with antibodies aimed at evaluating the activation status of the mTOR pathway. Data are representative of at least 3 independent experiments.

B   Clonogenic assay of HeLa cells in adherence. 250 HeLa cells KD for either GOLPH3 or LCS were allowed to form colonies for 10 days. Afterwards, colonies were fixed and stained as detailed in Materials and Methods. The graph on right reports the number of colonies per well in each indicated condition (data are means ± SEM of 3 independent experiments; *$P < 0.05$, **$P < 0.01$ [Student's t-test]).

C   Soft agar colony formation assay of HeLa cells transfected with different concentration of either GOLPH3 (left upper graph) or LCS (left bottom graph) encoding plasmids. Soft agar colony formation assay of HeLa cells KD for either GOLPH3 or LCS (right upper graph). Soft agar colony formation assay of HeLa cells KD for LCS and GOLPH3 OE alone or in combination with LCS KD (right bottom graph). Colonies were stained and quantified as described in Materials and Methods; (individual data points are shown in the graphs; data are means ± SD of at least three independent experiments; *$P < 0.05$, ***$P < 0.001$, n.s. = not significant [Student's t-test]).

D   Protein lysates from parental (left), GCS-KO (middle) and LCS-KO (right) HeLa cells, CTRL or GOLPH3-OE were processed for SDS–PAGE and WB with the indicated antibodies. Data are representative of at least three independent experiments.

E   Soft agar colony formation assay of parental and LCS-KO HeLa cells expressing LCS-HA or GOLPH3. Colony number was quantified; (individual data points are shown in the graphs; data are means ± SD of at least three independent experiments; ***$P < 0.001$ [Student's t-test]).

F   Quantification of soft agar colony formation assay of LNCaP and DU145 prostatic cancer cell lines treated with increasing concentrations of siRNA targeting GOLPH3 or LCS (data are means ± SEM of at least three independent experiments; ***$P < 0.001$ [Student's t-test]).

Source data are available online for this figure.

protein levels showed also high LCS protein levels (~65% of cases; Fig 6C and D), while only ~20% of the GOLPH3 weak or negative samples had moderate to high LCS expression levels (Fig 6C and D and in Table EV1). Overall, while a larger sample might be desirable for clinical conclusions, we find a significant (χ^2 $P < 0.0001$) correlation between GOLPH3 and LCS protein levels.

Our data that LCS OE phenocopies the signalling and proliferative effects of GOLPH3 pose the question of whether LCS itself can be endowed with oncogenic properties. The gene encoding LCS (i.e. *B4GALT5*) is located on the chromosomal region 20q13.13 that has been found amplified in multiple human cancers (Scotto *et al*, 2008; Han *et al*, 2013; Wang *et al*, 2015; Guo *et al*, 2017). Database [cBioPortal; http://www.cbioportal.org/; (Gao *et al*, 2013)] searches for alterations in *B4GALT5* gene in large patient cohorts show that *B4GALT5* is amplified in 11% and 7% of uterine and colorectal cancer samples, respectively. In these tumours, *B4GALT5* amplification correlates with higher mRNA levels (Fig EV4O and P). Moreover, *B4GALT5* has been reported to correlate with cancer cell stemness in breast tumours (Tang *et al*, 2020). Thus, based on our data, it is fair to hypothesise that LCS is an oncoprotein; nonetheless, this hypothesis needs to be tested in dedicated studies.

From the clinical standpoint, *GOLPH3* amplification has been associated with poor prognosis in several cancer types (Buschman *et al*, 2015). Searching the TCGA database (Gao *et al*, 2013) for data on *GOLPH3* relevance in cancer prognosis reveals that *GOLPH3* amplification strongly correlates with decreased disease-free survival (though not with decreased overall survival) both in overall TCGA cancer studies and specifically in lung squamous carcinoma (Fig EV4Q).

Discussion

The lipid composition of the PM plays fundamental roles in determining the subcellular localisation and the lateral segregation of integral and membrane-associated proteins, with paramount implications for cell signalling and physiology (van Meer *et al*, 2008; Holthuis & Menon, 2014). Bioactive GSLs are major functional components of the mammalian PM (Merrill, 2011; D'Angelo *et al*, 2013a; D'Angelo *et al*, 2013b). These are variably glycosylated sphingolipids synthesised by numerous enzymes organised in competing synthetic pathways and dynamically distributed across the stacked Golgi *cisternae* (D'Angelo *et al*, 2013a). Their assembly occurs during intra-Golgi transport, resulting in different GSL patterns in different cell types and tissues (D'Angelo *et al*, 2013a). The production of a given GSL profile depends on the sub-Golgi localisation and levels of GSL enzymes, their reaction rates (determined by the cisternal lumenal milieu), substrate availability and the association among enzymes to form multi-enzymatic complexes (D'Angelo *et al*, 2013a). These parameters are all controlled by Golgi trafficking machineries. Nevertheless, surprisingly, how intra-Golgi transport governs GSL metabolism has so far remained poorly understood.

In this study, we report, for the first time, some of the mechanistic principles by which intra-Golgi trafficking influences competing GSL metabolic pathways and the associated cellular functions. We find that a selected group of enzymes operating in the initial segment of the GSL synthetic pathways and at the branchpoint

between the complex GSL series interacts with the Golgi protein GOLPH3. GOLPH3 is a COPI adaptor (Tu *et al*, 2008; Eckert *et al*, 2014) endowed with oncogenic activity (Scott *et al*, 2009) that resides in the *trans* Golgi where it mediates the incorporation of GSL client enzymes into retrograde transport vesicles and, hence, promotes their retro-transport towards the proximal *cisternae*. Moreover, we find that GOLPH3 operates as a part of the cisternal progression inter-conversion process that supports the sub-Golgi localisation of glycoenzymes. Through these two properties GOLPH3 generates a cascade of effects of great functional relevance: A) it dictates the *trans* Golgi localisation of multiple GSL synthetic enzymes, B) it regulates the Golgi levels of these specific enzymes, C) it controls, through its client enzymes, the conversion of Cer into globo and ganglio series GSLs endowed with effects on cell growth. By influencing GSL metabolism, GOLPH3 controls mitogenic signalling and the proliferation of cancer cell. Below, we discuss some salient aspects of these results.

Mechanism of the GOLPH3-dependent localisation of GSL enzymes at the trans cisterna

As schematised in the model in Fig EV5A, the localisation of LCS and other GOLPH3 clients appears to be dictated by the localisation of GOLPH3 itself at the *trans* Golgi in the context of the cisternal maturation mechanism. GOLPH3 is recruited to the *trans* Golgi by PtdIns(4)P produced by the action of PtdIns transfer proteins (PITPs) and PI4KIIIB (Halberg *et al*, 2016; Xie *et al*, 2018; Tan *et al*, 2020). Once recruited, GOLPH3 binds and incorporates its client enzymes into COPI-dependent retrograde vesicles (Eckert *et al*, 2014) for transport to proximal *cisternae* (mostly the medial element). There, GOLPH3 detaches from the membranes, presumably because of a local decrease of PtdIns(4)P levels (De Matteis *et al*, 2013), and releases the enzymes. At the same time, the *trans* cisterna disassembles and the medial *cisterna* matures into a *trans* element and progresses forward to the *trans* position, where PtdIns(4)P is produced and GOLPH3 is recruited again to start a new enzyme transport round. As a result, GOLPH3 cycles between the *trans* and medial *cisternae*, with a prevalent steady-state localisation in the *trans* position, and drives client enzymes through the same cycle. How the PtdIns(4)P synthesis-degradation cycle links into the cisternal maturation mechanism, remains a subject for future investigations. We note that, while GOLPH3 has been shown to mediate enzyme retention in the Golgi, the mechanisms described here represent the first molecular model for the sub-Golgi localisation of any glycoenzyme. Similar mechanisms, based on the regulated localisation of an enzyme adaptor at a given *cisterna* by the cisternal maturation process, are likely to be involved in the localisation of many other Golgi enzymes.

It is also important to mention that the PtdIns(4)P pool at the *trans* Golgi (Mesmin *et al*, 2019) plays a role not only in the localisation of GOLPH3 but also in other functions of relevance for GSL metabolism. PtdIns(4)P recruits CERT and FAPP2, which deliver the GSL precursors Cer and GlcCer to the *trans* Golgi region for their metabolic conversion (Hanada *et al*, 2003; D'Angelo *et al*, 2007). Thus, by controlling both substrate provision (i.e. via CERT and FAPP2) and enzymes localisation (i.e. via GOLPH3) at the *trans* Golgi, PtdIns(4)P coordinates GSL metabolism at the Golgi complex (Fig EV5A).
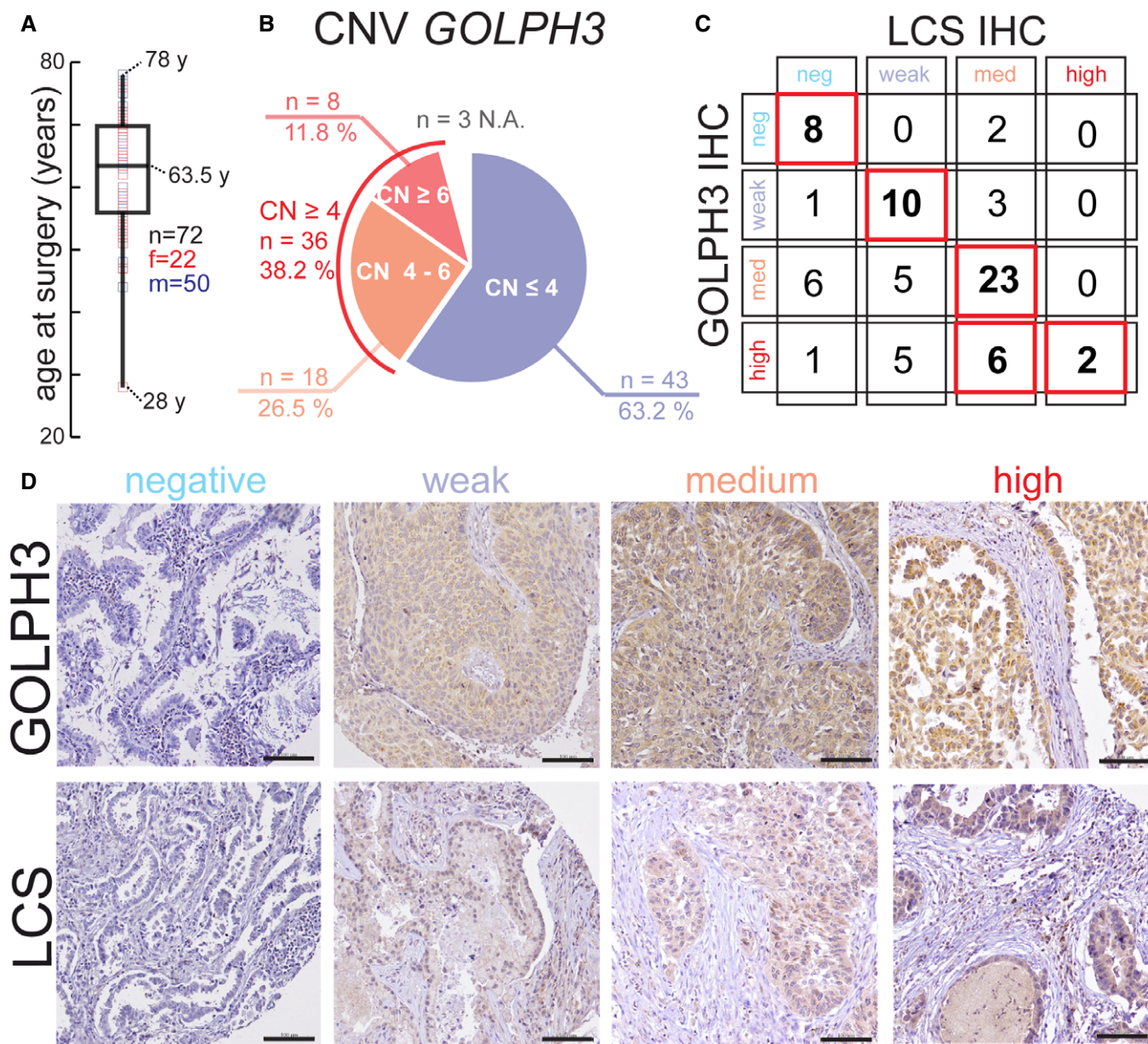
Figure 6. GOLPH3 and LCS protein levels correlate in NSCLC tissue samples.

A–C Surgical specimens were collected from 72 non-small cells lung cancer (NSCLC) patients. In (A) age at surgery and sex distribution of the patients are reported. Data are depicted as a box plot. The central band represents the mean ± quartiles, the whiskers mark the range. (B) Copy number (CN) variations in GOLPH3 gene were assessed in cancer tissue section by DNA FISH as described in Materials and Methods and are expressed as a pie chart. (C) Cancer tissue sections were processed for IHC using antibodies against endogenous GOLPH3 and LCS. The IHC intensity of the staining for each section and for both the tested proteins was classified according to the criteria described in Materials and Methods. A contingency table for the GOLPH3 and LCS staining is reported in Table EV1.

D Representative images of NSCLC sections stained for GOLPH3 and LCS. Scale bar, 100 μm.

Mechanisms of the GOLPH3 dependent regulation of the levels of GSL enzymes

While the cycling between *trans* and medial *cisternae* is an effective enzyme localisation mechanism, GOLPH3 clients can escape this cycle, depending on the levels of GOLPH3. This has important functional consequences. When GOLPH3 levels decrease, GOLPH3 clients are recycled inefficiently and leave the Golgi for the lysosomes, where they are degraded. When the GOLPH3 levels increase, the GOLPH3 clients are instead recycled and retained in the Golgi efficiently, which prevents their lysosomal degradation. As a result, GOLPH3 controls not only the localisation but also the levels of its clients. A crucial aspect of this degradation-based mechanism is that, at physiological GOLPH3 levels, Golgi enzyme retention is

suboptimal, which allows a fraction of the GSL enzymes to reach the lysosomes, resulting in the relatively fast degradation of the GOLPH3 clients. This makes the levels of these enzymes amenable to regulation by increases in GOLPH3 levels (see above). GOLPH3 can thus be seen as a rheostat that, by promoting the retrograde transport of its client enzymes, acts to reduce their anterograde flux towards the lysosomes, and in this way regulates their turnover, and levels (Fig EV5B).

Importantly, the fast degradation of GOLPH3 clients under basal conditions is not a peculiarity of HeLa cells. Data consistent with this observation have been obtained in human fibroblasts and are in line with results in prostate cancer cell lines and in cancers from human patients.

So far, the Golgi levels of glycoenzymes have been thought to be regulated by transcriptional means. The above described degradation-based regulation of the GSL enzymes represents a novel mechanism for the control of the Golgi enzyme levels.

GOLPH3 controls GSL metabolism and, as a consequence, cell proliferation

The overexpression of GOLPH3, which occurs in many human tumours, enhances the levels of GSL metabolic enzymes involved in two metabolic axes, one from LacCer to Gb3 and the other from LacCer to GM3 to GD3 (Fig EV5C). Both these pathways lead to activation of mitogenic signalling and cell growth. Our data indicate that, in HeLa cells, the GOLPH3 induced enhancement of the GCS-LCS-Gb3S GSL metabolic axis is responsible for the GOLPH3 mitogenic effects, while the GM3S to GD3S axis seems to play a negligible role. However, this is likely because the transcriptional expression of Gb3S is predominant in HeLa cells (Russo et al, 2018), and not because of a "preference" of GOLPH3 for this enzymatic pathway. In cell types and tissues where the expression of the ganglio series synthetic enzymes is prominent (e.g. in cell types of neural origin (Russo et al, 2018)), GOLPH3 is likely to promote ganglioside metabolism.

Regardless, the GOLPH3-dependent changes reprogram the GSL pathway towards a pro-growth configuration. The growth-inducing properties of specific globosides and gangliosides are known. Gb3 and its downstream metabolites Gb4 and sialyl-Gb5 cluster in GSL-rich domains at focal adhesions, where they bind to and activate integrins and RTK receptors to promote PI3K-Akt-mTOR signalling (Hakomori Si, 2002; Steelant et al, 2002; Park et al, 2012; Wegner et al, 2018; Chuang et al, 2019; Furukawa et al, 2019), and the ganglioside GD3 is a characterised activator of RTK receptors (Ohkawa et al, 2010). Moreover, a contributing factor to the GOLPH3-induced growth is probably the enhanced consumption of ceramide, a characterised tumour suppressor and inhibitor of cell proliferation (Reynolds et al, 2004; Hannun & Obeid, 2008; Fig EV5D). A complete analysis of the mitogenic effects of the GOLPH3-induced GSLs metabolites is a task for future work.

Are the oncogenic effects of GOLPH3 mediated exclusively by the observed changes in GSL metabolism? GOLPH3 is an extensively studied oncogene and several hypotheses have been previously put forward in the past to account for its effect on growth (Scott & Chin, 2010; Farber-Katz et al, 2014; Isaji et al, 2014; Halberg et al, 2016; Rizzo et al, 2017).

Our data indicate that the effect of GOLPH3 on pro-growth GSL metabolites represents a central component of the GOLPH3 mitogenic effects. However, in addition to the enzymes studied here, other GSL enzymes that bear the LxxR GOLPH3 recognition motif might be GOLPH3 clients and have a role in GOLPH3 function. It is also possible that the GOLPH3-controlled enzymatic module comprises enzymes unrelated to GSL metabolism. ST6GAL1, for instance, bears the LxxR motif in its tail and has been proposed to mediate the effect of GOLPH3 on cell migration by sialylating integrins (Isaji et al, 2014). Proteoglycan synthetic enzymes have been shown to play a role in tumorigenesis, and in Drosophila some of them are controlled by GOLPH3 (Chang et al, 2013). Moreover, Vps74p acts on some yeast enzymes that are devoid of the LxxR motif, expanding the range of the possible GOLPH3 clients (Wang et al, 2020). Finally, glycoenzyme-unrelated activities of GOLPH3 have been proposed to contribute to its oncogenic properties. Among these, the GOLPH3 effects on cargo export from the TGN and on the DNA damage response have been thoroughly characterised (Dippold et al, 2009; Farber-Katz et al, 2014; Halberg et al, 2016; Xie et al, 2018; Rahajeng et al, 2019) and shown to be relevant for cell proliferation. How these mechanisms synergise with the effects of GOLPH3 on GSL metabolism remains to be determined.

Conclusions and Perspectives

The current findings provide insight into the biosynthetic mechanisms of GSLs in the Golgi complex and open new research avenues in the area of sphingolipid metabolism. As noted, in addition to the enzymes studied here, several other GSL biosynthetic enzymes, involved in other biosynthetic pathways, are likely to be GOLPH3 clients and remain to be studied. Moreover, enzymes of GSL metabolic pathways that are independent of GOLPH3, such as those involved in the synthesis of lacto and asialo GSL series, are probably controlled by adaptors that are functionally analogous to GOLPH3 and may now be characterised using experimental strategies similar to those used for GOLPH3.

Taking a broader perspective, the current study on GSL synthesis can impact on our understanding of the mechanisms of glycosylation in general, rather than only of sphingolipid glycosylation. GSL biosynthesis is a convenient model for glycosylation studies because of the relative structural simplicity of the GSLs, the presence of known critical branchpoints in the GSL metabolic networks, and the fact that the glycan portion is the major determinant of the function of the GSLs. These characteristics have therefore allowed us to address issues that are relevant for all glycosylation pathways. These are the localisation mechanisms of glycoenzymes in specific Golgi cisternae; the regulation of the degradation, and hence the levels, of Golgi enzymes by the Golgi; the organisation, mediated by specific adaptors, of the glycoenzymes into functionally coherent modules capable of regulating specific cellular functions. The analysis of the Golgi mechanisms of GSL biosynthesis may provide a blueprint for studies of other glycosylation pathways.

The last point, in particular, carries special significance in that it suggests that multiple enzyme recycling modules operate separately in the maturation of mammalian Golgi cisternae. This idea requires a revision of the previous concept of cisternal maturation. The cisternal maturation process, based on Golgi enzyme recycling, has

so far been considered a constitutive process functioning merely to maintain the constancy of the enzymatic composition of *cisternae* during intra-Golgi cisternal progression. Our finding that GOLPH3 drives selectively the recycling of a functionally coherent enzymatic module, with a regulatory impact on cell growth, and not of other enzymes, supports a more complex scenario in which the cisternal maturation process is a mosaic of recycling enzyme modules (*i.e.* driven by specific adaptors) acting to modulate the glycan outputs of various glycosylation pathways. This has never been proposed before, although it is, in fact, supported by a few earlier observations (Tu *et al*, 2008; Liu *et al*, 2018). This organisation of intra-Golgi transport can have major functional consequences and may provide a useful framework for future studies of glycosylation.

On a more translational ground, our data indicate that the Golgi mechanisms underlying GSL biosynthesis described here can have consequences in physiology and pathology and do, in fact, operate in tumours of human patients. GOLPH3 and its upstream regulators (*i.e.* the *trans* Golgi located PtdIns(4)P signalling circuit) are emerging as clinically relevant entities in a number of frequent and poorly treatable human cancers (Scott *et al*, 2009; Halberg *et al*, 2016; Tan *et al*, 2020). The current findings on the oncogenic mechanism of GOLPH3 (and possibly of oncogenes that rely on GOLPH3 for their activity (Halberg *et al*, 2016; Tan *et al*, 2020)) are bound to have significant medical and pharmacological relevance.

Materials and Methods

Contact for reagents and resource sharing

Further information and requests for resources and reagents should be directed to and will be fulfilled by the Lead Contacts: Alberto Luini (alberto.luini@ibbc.cnr.it) and Giovanni D'Angelo (giovanni.dangelo@epfl.ch).

Cell lines and culture conditions

HeLa-M (human cervical cancer cells, female origin) were obtained from the ATCC. DU145 (prostate cancer cells, human male origin) were a kind gift from Carmen Valente from the Institute of Biochemistry and Cell Biology, CNR, Naples. LNCaP cells (prostate cancer cells, human male origin) were a kind gift from Alfredo Budillon from the Istituto Nazionale Tumori "Fondazione Pascale". HeLa-M, DU145 and LNCaP cells were cultured in RPMI-1640 medium containing 4.5 g/l glucose, 2 mM L-glutamine, 10% foetal calf serum (FCS), and 100 U/ml penicillin and streptomycin. Primary human fibroblasts (PHFs) (normal cells, male origin) were obtained from the Telethon Biobank. The HeLa-mCAT#8 (including TALEN UGCG-KO, and LCS-KO) cell lines (human cervical cancer cells, female origin) were kind gifts from Kentaro Hanada. Primary human fibroblasts, HeLa-mCAT#8, UGCG-KO and LCS-KO were cultured in DMEM containing 4.5 g/l glucose, 2 mM L-glutamine, 10% FCS, and 100 U/ml penicillin and streptomycin. Cells were grown under controlled temperature and atmosphere.

Plasmids and siRNA transfection

HeLa cells and PHFs were transfected with Mirus or Lipofectamine® LTX transfection reagents following the manufacturer's instructions

(1% FCS in HF medium). Oligofectamine was used for siRNA transfection and performed according to manufacturer's instructions (used at concentrations between 5 and 50 nM for the target gene). Each individual siRNA in the pool was also tested in localisation and signalling experiments. The list of siRNA sequences can be found in Appendix Table S1.

Immunoprecipitation and peptide pull-down assay

For co-immunoprecipitation experiments, HeLa cells were transfected with LCS-HA, cultured for 24 h and then lysed on ice with immunoprecipitation buffer (150 mM NaCl, 1% Igepal, 20 mM Tris–HCl, pH 7.4, protease inhibitors). The lysate was cleared and quantitated using the BCA Protein Assay kit (Pierce). Equal amounts of proteins were incubated with magnetic beads conjugated with anti-HA antibody (Sigma) overnight at 4°C. Then, the samples were washed extensively with immunoprecipitation buffer, eluted with HA peptide (Sigma), and analysed by SDS–PAGE and immunoblotting with anti-HA and anti-GOLPH3 antibodies (see Appendix Table S4).

Biotinylated N-terminal amino acid tails of Golgi enzymes were resuspended in 150 mM NaCl and 20 mM Tris pH 7.4. For each sample, between 1 and 5 µg of peptide was incubated with 40 µl of pre-washed monomeric avidin beads (Pierce) and incubated 1 h at 4°C. Beads functionalised with CTs were mixed with 500 µg of HeLa cell lysate (lysis buffer contains 150 mM NaCl, 20 mM Tris–HCl pH 7.4, 0.1% triton X-100, 1 mM DTT, protease and phosphatase inhibitors and 5 mM EDTA) or 5 µg of purified GOLPH3-His and incubated overnight at 4°C. Then, the samples were washed extensively with lysis buffer and analysed by SDS–PAGE and immunoblotting with anti-His or anti-GOLPH3 antibody (see Appendix Table S4).

Immunofluorescence and confocal microscopy

Cells grown on coverslips were fixed with 4% paraformaldehyde and permeabilised with 0.2% saponin (as described in (Trucco *et al*, 2004). Samples were then incubated with selected antibodies against the antigen of interest at 4°C overnight followed by second antibodies labelled with Alexa Fluor dyes (Invitrogen). The coverslips were then mounted and analysed under a confocal microscope [LSM700; Carl Zeiss; 40× or 63 × oil-immersion objective (1.4 NA)]. Images were processed using Metamorph 7.7.3.0 (Universal Imaging) and ImageJ software. Excel and GraphPad Prism version 5.0 software were used for data analyses and graphing. Adobe Photoshop CS3 was used to adjust the contrast of the images (for presentation only), whereas Adobe Illustrator CC 2014 (Adobe Systems) was used to illustrate figures and draw models.

Live cell imaging

For live cell imaging, HeLa-M cells transiently expressing LCS-GR (for brevity indicated in the text as GFP-GR) were grown on glass-bottomed 35-mm dishes which were then mounted on a Zeiss LSM700 laser scanning microscope under controlled temperature and CO_2. The images were acquired at regular interval (488 for excitation; PMT: 510–550 nm; 512 × 512 pixels; frame average, 4).

Immunoelectron microscopy

The samples were fixed and processed as described previously (Rizzo *et al*, 2013). In brief, HeLa cells were fixed with 4% paraformaldehyde and 0.05% glutaraldehyde for 30 min at room

temperature, then washed with PBS/0.02 M glycine and embedded in 12% gelatin in PBS. Small blocks (1 mm) were obtained and infiltrated with 2.3 M sucrose at 4°C. Ultrathin cryosections (50–70 nm) were prepared using a UC7 Leica cryo-ultramicrotome and incubated with indicated antibodies of interest followed by protein A gold. Random sampling of Golgi stacks was performed using a Tecnai-12, FEI transmission electron microscope, and pictures were acquired using a Veletta CCD digital camera. Morphological (clathrin at the TGN) and compositional (*cis* Golgi marker GM130) criteria were used to define the polarity of the Golgi stacks. For quantitation (performed with iTEM image acquisition software) *cis*, medial or *trans* Golgi were defined as previously described (Rizzo *et al*, 2013). *Cis* indicated the *cis*-most *cisterna* in the case of a stack with three or four *cisternae*, and the two *cis*-most *cisternae* in the case of a stack with five *cisternae* (here, the LD was the mean of the two). *Trans* was the last (*trans*) *cisterna*. Medial was the remaining one or two central *cisternae*. Vesicles were round profiles of 50–80 nm in diameter, present within 200 nm of the rims of the stack. The distribution of LCS-HA, GalT1 and GOLPH3 within the Golgi stacks was expressed as linear density (LD), which represents the number of gold particles/μm.

Proliferation assays

For in adherence colony formation assays, after treatment, 250 cells for each condition were seeded into 6-well plates and grown for 10 days. Cell colonies were glutaraldehyde-fixed and stained with crystal violet (0.1 % w/v) for 10 min, washed with water and counted using ImageJ software. Soft agar growth assays were performed on 12-well plates in triplicate. For each well, 1×10^4 cells were mixed thoroughly in cell growth medium containing 0.3% agarose (Invitrogen, 16500-500) in DMEM plus 10% FCS, 1% penicillin/streptomycin, and 0.5 mM sodium pyruvate, followed by plating onto bottom agarose prepared with 0.6% agarose in DMEM and 10% FCS. The wells were allowed to solidify, and 200 μl of growth medium was added on top and refreshed every 4 or 5 days to avoid agar drying. After 10–30 days, depending on the cell line, colonies were stained with nitrotetrazolium blue chloride (Sigma N6876), scanned, and counted using ImageJ.

Experimental conditions for LCS-GR traffic assay

1   GOLPH3-KD HeLa cells were transiently transfected with LCS-GFP_RUSH (referred as LCS-GR in the text) at 37°C in absence of biotin. Cells were then treated with nocodazole (33 μM) and cycloheximide (50 mg/ml) for 3 h prior to shifting the temperature to 10°C for 60 min in the presence of biotin (40 μM). Then, cells were re-shifted to 37°C for the indicated times (Appendix Table S5), fixed and subjected to IF. See Appendix Table S5 for a scheme of the synchronisation protocol.

2   GOLPH3-KD HeLa cells were transiently transfected with LCS-GR and culture at 37°C in the absence of biotin for 24 h. Cells were then infected with VSV-G and cultured at 40°C for 3 h in presence of nocodazole (33 μM), prior to shifting the temperature to 10°C for 60 min in presence of biotin (40 μM) and cycloheximide (50 mg/ml). Then, cells were re-shifted to 32°C for the indicated time, fixed and subjected to IF. See Appendix Table S5 for a scheme of the synchronisation protocol.

Lipid analysis

(Glyco)sphingolipid measurements
HPLC-mass spectrometry

Glycophingolipids were analysed by liquid chromatography-tandem mass spectrometry (LC-MS/MS) as described earlier (Bielawski *et al*, 2006). Briefly, extracts were analysed with a Quantum Ultra triple quadrupole mass spectrometer connected to an Accela HPLC and Accela autosampler using a solvent gradient. Ceramides identity was achieved through MRM analysis with soft fragmentation. Quantitative analysis is based on calibration curves generated for each lipid. Levels of SLs were normalised to inorganic phosphate (Pi) released from total phospholipids.

HPTLC

Cells were pulse-labelled with 0.1 μCi/ml ($\approx$ 5 nM) ^{3}H-D-erythro-Sphingosine for 2 h and chased for the indicated times. Subsequently, cells were harvested and processed for lipid extractions. Lipids were spotted on silica-gel high-performance TLC (HPTLC) plates (Merck, Germany) and resolved with a mixture of chloroform: methanol: water (65:25:4 v/v/v). To visualise the unlabelled standards (*i.e.* Cer, GlcCer, LacCer, Gb3, GM3 and SM), the TLC plates were placed in a sealed tank saturated with iodine vapours, while the radiolabelled lipids were analysed using a RITA$^{\circledR}$ TLC Analyser (Raytest, Germany), and quantified using GINA$^{\circledR}$ (Raytest, Germany) software analysis. The percentage of total C.P.M. associated with each sphingolipid are reported as percentage of total sphingolipids.

MALDI-MS
Lipid extraction

Total lipid extracts were prepared using a standard MTBE protocol followed by a methylamine treatment for sphingo- and GSL analysis by mass spectrometry. Briefly, cell pellet was resuspended in 100 μl H_2O. 360 μl methanol and 1.2 ml of MTBE were added and samples were placed for 10 min on a vortex at 4°C followed by incubation for 1 h at room temperature on a shaker. Phase separation was induced by addition of 200 μl of H_2O. After 10 min at room temperature, samples were centrifuged at 1,000 g for 10 min. The upper (organic) phase was transferred into a glass tube, and the lower phase was re-extracted with 400 μl artificial upper phase [MTBE/methanol/H_2O (10:3:1.5, v/v/v)]. The combined organic phases were dried in a vacuum concentrator. Lipids were then resuspended in 500 μl of $CHCl_3$ and divided in two aliquots for a further methylamine treatment. 500 μl of freshly prepared monomethylamine reagent [methylamine/H_2O/n-butanol/methanol (5:3:1:4, (v/v/v/v)] was added to the dried lipid extract and then incubated at 53°C for 1 h in a water bath. Lipids were cooled to room temperature and then dried. The dried lipid extract was then extracted by n-butanol extraction using 300 μl water-saturated n-butanol and 150 μl H_2O. The organic phase was collected, and the aqueous phase was re-extracted twice with 300 μl water-saturated n-butanol. The organic phases were pooled and dried in a vacuum concentrator. Lipids were then resuspended in 500 μl of $CHCl_3$ and analysed by MALDI-MS. 30 mg/ml 2,5-DHB was freshly prepared in acetonitrile/water solution (50:50 v/v) with 0.1% TFA. An equivalent volume of sample solution (50 μl) was then mixed with matrix before deposition on the MALDI target. All mass spectrometry analyses for the

identification of lipids (m/z 600-1,800) were obtained using an Applied Biosystems 4800 MALDI-TOF/TOF mass spectrometer equipped with a 200 Hz tripled-frequency Nd:YAG pulsed laser with 355 nm wavelength. Measurements were performed in positive ion reflection mode at an accelerating potential of 20 kV. Each mass spectra were obtained by applying a laser energy of 4,600 watts/cm^2, averaging 4,000 single laser shots/spectrum.

Untargeted Lipidomics

For phospholipid analysis, lipid extracts (2 µl injection volume in CHCl$_3$:MeOH 2:1) were separated over an 8-minute gradient at a flow rate of 200 µl/min on a HILIC Kinetex Column (2.6lm, 2.1 × 50 mm^2) on a Shimadzu Prominence UFPLC xr system (Tokyo, Japan). Mobile phase A was acetonitrile:methanol 10:1 (v/v) containing 10 mM ammonium formate and 0.5% formic acid, while mobile phase B was deionised water containing 10 mM ammonium formate and 0.5% formic acid. The elution of the gradient began with 5% B at a 200 µl/min flow and increased linearly to 50% B over 7 min; then the elution continued at 50% B for 1.5 min, and finally, the column was re-equilibrated for 2.5 min. MS data were acquired in full-scan mode at high resolution on a hybrid Orbitrap Elite (Thermo Fisher Scientific, Bremen, Germany). The system was operated at 240,000 resolution (m/z 400) with an AGC set at 1.0E6 and one microscan set at 10 msec maximum injection time. The heated electrospray source HESI II was operated in positive mode at a temperature of 90°C and a source voltage at 4.0 KV. Sheath gas and auxiliary gas were set at 20 and 5 arbitrary units, respectively, while the transfer capillary temperature was set to 275°C.

Isothermal titration calorimetry (ITC)

ITC experiments were performed in a buffer containing 300 mM NaCl, 10 mM Bicine pH 8.5 and 1 mM DTT. LCS Peptides were synthesised and delivered as lyophilised powder with a biotin moiety located at the N-terminus (Charite Universitaetsmedizin Berlin, Germany). The peptides were dissolved in buffer, centrifuged at 14,000 *g* for 10 min, and only the supernatant was used. The dissolved peptide concentrations were calculated based upon their absorbance at 280 nm and their corresponding molar extinction coefficient. Experiments consisted of titrations of 20 injections of 2 µl of titrant (peptides) into the cell containing GOLPH3 protein at a 25-fold lower concentration. Typical concentrations for the titrant were around 2.5 mM for experiments depending on the affinity. Experiments were performed at 25°C and a stirring speed of 1,000 rpm on a MicroCal PEAQ-ITC (Malvern Panalytic). All data were processed using MicroCal PEAQ-ITC Analysis Software and fit to a one-site binding model after background buffer subtraction.

TMA Building

72 surgical specimens from non-small cell lung cancer (NSCLC) patients collected from 2006 to 2010, at the National Cancer Institute "Giovanni Pascale" of Naples, were used for building a tissue microarray (TMA). The TMA was built using two cores from different areas selected on the H&E-stained slides and, whenever possible, one core of normal tissue of the same tissue block. Tissue cylinders with a diameter of 1 mm were punched from morphologically representative tissue areas of each "donor" tissue block and brought into one recipient paraffin block (3 × 2.5 cm) using a semi-automated tissue arrayer (Galileo TMA).

Immunohistochemistry

A standard protocol was used for the immunostaining of the paraffin embedded samples to evaluate the expression of GOLPH3 and LCS; an appropriate external positive control tissue was used for each staining procedure; the negative control consisted of performing the entire IHC procedure on an adjacent section in the absence of the primary antibody. Briefly, paraffin slides (4 µm) were cut, deparaffinised in xylene and rehydrated through graded alcohols. Antigen retrieval was performed according to *manufacturer's instructions*, with slides heated in high pH solution (Dako EnVision FLEX Target Retrieval Solution 50×) for LCS and in low pH solution (Dako EnVision FLEX Target Retrieval Solution 50×) for GOLPH3, in a bath for 20 min at 97°C. The endogenous peroxidase was inactivated with 3% hydrogen peroxide, and then, the protein block (BSA 5% in PBS 1×) was performed. TMAs sections were incubated with the primary antibodies according to the specific conditions tested: anti-GOLPH3 (Polyclonal Rabbit-, Abcam Cat # ab98023 RRID: AB_10860828 – dilution 1:50, incubated 1 h) and anti-LCS (B4GALT5) (Monoclonal Mouse antibody-Clone 6D4-Kind gift from Henrik Clausen, Denmark—incubated 1 h). The tissue sections were incubated with IgG biotinylated secondary antibodies for 40 min at room temperature. Immunoreactivity was visualised by means of avidin-biotin-peroxidase complex kit reagents (Novocastra, Newcastle, UK) as the chromogenic substrate. Finally, the sections were developed with diaminobenzidine and counterstained with haematoxylin. Stained slides were analysed using an optical microscope (Olympus BX41). Expressions of the biomarkers were evaluated semi quantitatively based on the staining intensity and the number of immunoreactive cells. First, cytoplasmic-staining intensity was scored as follows: no staining (score 0), weak expression cytoplasmatic staining (score 1), moderate expression cytoplasmatic staining (score 2), high expression cytoplasmatic staining (score 3). Second, the percentage of positive cells was scored: no positive cells (0), 10% positive cells or less (1), 11% to 50% positive cells (2), 51% to 75% positive cells (3), and more than 75% positive cells (4). The immunoreactivity scores of the cancer tissue samples were determined based on the staining intensity and area of positive staining according to the method used by (Wang et al, 2014).

Fish assay

FISH for GOLPH3 status was performed on TMA section using a mix of two probes according to the manufacturer's instructions, one labelled Orange to detect GOLPH3 (5p13.3) and ones Green to Chromosome 5 control probe (5p11) (Empiregenomics). Briefly, TMA was cut in 5 µm thick sections. The slides were baked for 1 h at 60°C and then placed in a solution for deparaffination followed by dehydration steps. The slides were treated with protease solution and pretreatment with a commercial kit (Paraffin pretreatment reagent kit; Vysis) on the half-automated VP2000 processor system (Abbott Molecular, Wiesbaden, Germany). After pretreatment, the slides were denatured with the mixture of probes for 5 min at 85°C and hybridised at 37°C overnight in a Thermobrite (Leica). Post-hybridisation 2XSSC 0.1% NP40 washes were performed both at room temperature and 72°C; then, the slides were stained with DAPI before analysis. Normal tissue and lymphocytes were considered as internal controls. Tumour core tissue was entirely scanned for amplification by using a 63 objective and appropriate filter sets (BX61 fluorescent microscope; Olympus). If GOLPH3 signal showed

a homogenous distribution, random areas were used for counting the signals. Each FISH slide was evaluated by 2 independent investigators in a blind manner. A minimum of 40 nuclei were counted on each spot. Amplification of GOLPH3 was defined when GOLPH3/ Centromere 5 ratio was ≥ 2.0 or when the average of GOLPH3 signals for cell was ≥ 6.0. The copy number gain was considered when the average of GOLPH3/cell signals were > 4.0 and < 6.0.

Quantification and statistical analysis

Error bars correspond to either standard deviation (SD) or standard error of the mean (SEM) according to the different experiments and as indicated in the figure legends. Statistical evaluations report on Student's *t*-test $^*P < 0.05$, $^{**}P < 0.01$ and $^{***}P < 0.001$ (ns, not significant).

Data availability

Targeted lipidomics data from this study are available at Metabolomics Workbench database with the following IDs: ST001673 for HeLa cells, and ST001672 for PHFs. Untargeted lipidomics data from this study are available at Metabolomics Workbench database with the following ID: ST001674.

Expanded View for this article is available online.

Author contributions

RR developed the idea, conducted most of the experiments and contributed to the writing of the manuscript; DR participated in the development of the idea and conducted most of the experiments and contributed to the writing of the manuscript; KK conducted the experiments with yeast cells; PS conducted the GalT1-RUSH experiment and contributed to cell signalling and proliferation experiments; BL was involved in the setup of the RUSH synchronisation protocol of LCS-GFP_RUSH and EM assessment of GOLPH3 distribution; DS assisted RR in conducting the experiments at the initial phase of the project; MAZ conducted bioinformatics analysis of Golgi enzyme tails; AV conducted the ITC experiments; PP and VK assisted RR in conducting the experiments at the final phase of the project; LC conducted MALDI-MS and lipidomics measurements; GB and FP generated RUSH constructs; FZM, GA and CV conducted TMA experiment; PH generated biotinylated peptides; LM expressed and purified recombinant GOLPH3; DM assisted RR in conducting the experiments at the initial phase of the project; GB and AB analysed and interpreted the TMA data; HC and UM generated and provided LCS antibody and analysed glycosylation data; TY and KH generated and provided the GCS- and LCS-KO HeLa cells; SP contributed to conception and design, analysis and interpretation of data and contributed to the writing of the manuscript; YAH helped with analysis and interpretation of lipids MS data and contributed to write the manuscript; AN was involved in data analysis and interpretation of experiments with yeast cells; DC contributed to development of the idea and to the critical analysis of the data throughout the entire project; GDA and AL developed the idea, designed and supervised the entire project, and wrote the manuscript.

Conflict of interest

The authors declare that they have no conflict of interest.

References

Ali MF, Chachadi VB, Petrosyan A, Cheng PW (2012) Golgi phosphoprotein 3 determines cell binding properties under dynamic flow by controlling Golgi localization of core 2 N-acetylglucosaminyltransferase 1. *J Biol Chem* 287: 39564−39577

Bielawski J, Szulc ZM, Hannun YA, Bielawska A (2006) Simultaneous quantitative analysis of bioactive sphingolipids by high-performance liquid chromatography-tandem mass spectrometry. *Methods* 39: 82−91

Boncompain G, Divoux S, Gareil N, de Forges H, Lescure A, Latreche L, Mercanti V, Jollivet F, Raposo G, Perez F (2012) Synchronization of secretory protein traffic in populations of cells. *Nat Methods* 9: 493−498

Bonfanti L, Mironov Jr AA, Martinez-Menarguez JA, Martella O, Fusella A, Baldassarre M, Buccione R, Geuze HJ, Mironov AA, Luini A (1998) Procollagen traverses the Golgi stack without leaving the lumen of cisternae: evidence for cisternal maturation. *Cell* 95: 993−1003

Bonifacino JS, Glick BS (2004) The mechanisms of vesicle budding and fusion. *Cell* 116: 153−166

Breton C, Snajdrova L, Jeanneau C, Koca J, Imberty A (2006) Structures and mechanisms of glycosyltransferases. *Glycobiology* 16: 29R−37R

Buschman MD, Rahajeng J, Field SJ (2015) GOLPH3 links the Golgi, DNA damage, and cancer. *Cancer Res* 75: 624−627

Casler JC, Papanikou E, Barrero JJ, Glick BS (2019) Maturation-driven transport and AP-1-dependent recycling of a secretory cargo in the Golgi. *J Cell Biol* 218: 1582−1601

Chang WL, Chang CW, Chang YY, Sung HH, Lin MD, Chang SC, Chen CH, Huang CW, Tung KS, Chou TB (2013) The *Drosophila* GOLPH3 homolog regulates the biosynthesis of heparan sulfate proteoglycans by modulating the retrograde trafficking of exostosins. *Development* 140: 2798−2807

Chuang PK, Hsiao M, Hsu TL, Chang CF, Wu CY, Chen BR, Huang HW, Liao KS, Chen CC, Chen CL *et al* (2019) Signaling pathway of globo-series glycosphingolipids and beta1,3-galactosyltransferase V (beta3GalT5) in breast cancer. *Proc Natl Acad Sci USA* 116: 3518−3523

D'Angelo G, Capasso S, Sticco L, Russo D (2013a) Glycosphingolipids: synthesis and functions. *FEBS J* 280: 6338−6353

D'Angelo G, Polishchuk E, Di Tullio G, Santoro M, Di Campli A, Godi A, West G, Bielawski J, Chuang CC, van der Spoel AC *et al* (2007) Glycosphingolipid synthesis requires FAPP2 transfer of glucosylceramide. *Nature* 449: 62−67

D'Angelo G, Uemura T, Chuang CC, Polishchuk E, Santoro M, Ohvo-Rekila H, Sato T, Di Tullio G, Varriale A, D'Auria S *et al* (2013b) Vesicular and

non-vesicular transport feed distinct glycosylation pathways in the Golgi. *Nature* 501: 116–120

Dippold HC, Ng MM, Farber-Katz SE, Lee SK, Kerr ML, Peterman MC, Sim R, Wiharto PA, Galbraith KA, Madhavarapu S et al (2009) GOLPH3 bridges phosphatidylinositol-4- phosphate and actomyosin to stretch and shape the Golgi to promote budding. *Cell* 139: 337–351

Eckert ES, Reckmann I, Hellwig A, Rohling S, El-Battari A, Wieland FT, Popoff V (2014) Golgi phosphoprotein 3 triggers signal-mediated incorporation of glycosyltransferases into coatomer-coated (COPI) vesicles. *J Biol Chem* 289: 31319–31329

Emr S, Glick BS, Linstedt AD, Lippincott-Schwartz J, Luini A, Malhotra V, Marsh BJ, Nakano A, Pfeffer SR, Rabouille C et al (2009) Journeys through the Golgi–taking stock in a new era. *J Cell Biol* 187: 449–453

Farber-Katz SE, Dippold HC, Buschman MD, Peterman MC, Xing M, Noakes CJ, Tat J, Ng MM, Rahajeng J, Cowan DM et al (2014) DNA damage triggers Golgi dispersal via DNA-PK and GOLPH3. *Cell* 156: 413–427

Fekry B, Jeffries KA, Esmaeilniakooshkghazi A, Szulc ZM, Knagge KJ, Kirchner DR, Horita DA, Krupenko SA, Krupenko NI (2018) C16-ceramide is a natural regulatory ligand of p53 in cellular stress response. *Nat Commun* 9: 4149

Furukawa K, Ohmi Y, Ohkawa Y, Bhuiyan RH, Zhang P, Tajima O, Hashimoto N, Hamamura K, Furukawa K (2019) New era of research on cancer-associated glycosphingolipids. *Cancer Sci* 110: 1544–1551

Gao J, Aksoy BA, Dogrusoz U, Dresdner G, Gross B, Sumer SO, Sun Y, Jacobsen A, Sinha R, Larsson E et al (2013) Integrative analysis of complex cancer genomics and clinical profiles using the cBioPortal. *Sci Signal* 6: pl1

Gill DM, King CA (1975) The mechanism of action of cholera toxin in pigeon erythrocyte lysates. *J Biol Chem* 250: 6424–6432

Glick BS, Nakano A (2009) Membrane traffic within the Golgi apparatus. *Annu Rev Cell Dev Biol* 25: 113–132

Godi A, Pertile P, Meyers R, Marra P, Di Tullio G, Iurisci C, Luini A, Corda D, De Matteis MA (1999) ARF mediates recruitment of PtdIns-4-OH kinase-β and stimulates synthesis of PtdIns(4,5)P2 on the Golgi complex. *Nature Cell Biology* 1: 280–287.

Goud B, Liu S, Storrie B (2018) Rab proteins as major determinants of the Golgi complex structure. *Small GTPases* 9: 66–75

Guo ST, Guo XY, Wang J, Wang CY, Yang RH, Wang FH, Li XY, Hondermarck H, Thorne RF, Wang YF et al (2017) MicroRNA-645 is an oncogenic regulator in colon cancer. *Oncogenesis* 6: e335

Hakomori SI (2008) Structure and function of glycosphingolipids and sphingolipids: recollections and future trends. *Biochim Biophys Acta* 1780: 325–346

Hakomori Si SI (2002) The glycosynapse. *Proc Natl Acad Sci USA* 99: 225–232

Halberg N, Sengelaub CA, Navrazhina K, Molina H, Uryu K, Tavazoie SF (2016) PITPNC1 recruits RAB1B to the Golgi network to drive malignant secretion. *Cancer Cell* 29: 339–353

Han J, Kim YL, Lee KW, Her NG, Ha TK, Yoon S, Jeong SI, Lee JH, Kang MJ, Lee MG et al (2013) ZNF313 is a novel cell cycle activator with an E3 ligase activity inhibiting cellular senescence by destabilizing p21(WAF1.). *Cell Death Differ* 20: 1055–1067

Hanada K, Kumagai K, Yasuda S, Miura Y, Kawano M, Fukasawa M, Nishijima M (2003) Molecular machinery for non-vesicular trafficking of ceramide. *Nature* 426: 803–809

Hannun YA, Obeid LM (2008) Principles of bioactive lipid signalling: lessons from sphingolipids. *Nat Rev Mol Cell Biol* 9: 139–150

Holthuis JC, Menon AK (2014) Lipid landscapes and pipelines in membrane homeostasis. *Nature* 510: 48–57

Isaji T, Im S, Gu W, Wang Y, Hang Q, Lu J, Fukuda T, Hashii N, Takakura D, Kawasaki N et al (2014) An oncogenic protein Golgi phosphoprotein 3 up-regulates cell migration via sialylation. *J Biol Chem* 289: 20694–20705

Ishii M, Suda Y, Kurokawa K, Nakano A (2016) COPI is essential for Golgi cisternal maturation and dynamics. *J Cell Sci* 129: 3251–3261

Jacewicz M, Clausen H, Nudelman E, Donohue-Rolfe A, Keusch GT (1986) Pathogenesis of shigella diarrhea. XI. Isolation of a shigella toxin-binding glycolipid from rabbit jejunum and HeLa cells and its identification as globotriaosylceramide. *J Exp Med* 163: 1391–1404

Jackson CL, Bouvet S (2014) Arfs at a glance. *J Cell Sci* 127: 4103–4109

Jeckel D, Karrenbauer A, Burger KN, van Meer G, Wieland F (1992) Glucosylceramide is synthesized at the cytosolic surface of various Golgi subfractions. *J Cell Biol* 117: 259–267

Kroesen BJ, Pettus B, Luberto C, Busman M, Sietsma H, de Leij L, Hannun YA (2001) Induction of apoptosis through B-cell receptor cross-linking occurs via de novo generated C16-ceramide and involves mitochondria. *J Biol Chem* 276: 13606–13614

Levy M, Futerman AH (2010) Mammalian ceramide synthases. *IUBMB Life* 62: 347–356

Liu L, Doray B, Kornfeld S (2018) Recycling of Golgi glycosyltransferases requires direct binding to coatomer. *Proc Natl Acad Sci USA* 115: 8984–8989

Losev E, Reinke CA, Jellen J, Strongin DE, Bevis BJ, Glick BS (2006) Golgi maturation visualized in living yeast. *Nature* 441: 1002–1006

Majumder S, Kono M, Lee YT, Byrnes C, Li C, Tuymetova G, Proia RL (2020) A genome-wide CRISPR/Cas9 screen reveals that the aryl hydrocarbon receptor stimulates sphingolipid levels. *J Biol Chem* 295: 4341–4349

Marks DL, Dominguez M, Wu K, Pagano RE (2001) Identification of active site residues in glucosylceramide synthase. A nucleotide-binding catalytic motif conserved with processive beta-glycosyltransferases. *J Biol Chem* 276: 26492–26498

Matsuura-Tokita K, Takeuchi M, Ichihara A, Mikuriya K, Nakano A (2006) Live imaging of yeast Golgi cisternal maturation. *Nature* 441: 1007–1010

De Matteis MA, Wilson C, D'Angelo G (2013) Phosphatidylinositol-4-phosphate: the Golgi and beyond. *BioEssays* 35: 612–622

van Meer G, Voelker DR, Feigenson GW (2008) Membrane lipids: where they are and how they behave. *Nat Rev Mol Cell Biol* 9: 112–124

Merrill Jr AH (2011) Sphingolipid and glycosphingolipid metabolic pathways in the era of sphingolipidomics. *Chem Rev* 111: 6387–6422

Mesmin B, Kovacs D, D'Angelo G (2019) Lipid exchange and signaling at ER-Golgi contact sites. *Curr Opin Cell Biol* 57: 8–15

Mironov AA, Beznoussenko GV, Nicoziani P, Martella O, Trucco A, Kweon HS, Di Giandomenico D, Polishchuk RS, Fusella A, Lupetti P et al (2001) Small cargo proteins and large aggregates can traverse the Golgi by a common mechanism without leaving the lumen of cisternae. *J Cell Biol* 155: 1225–1238

Mironov AA, Weidman P, Luini A (1997) Variations on the intracellular transport theme: maturing cisternae and trafficking tubules. *J Cell Biol* 138: 481–484

Nakano A, Luini A (2010) Passage through the Golgi. *Curr Opin Cell Biol* 22: 471–478

Ohkawa Y, Miyazaki S, Hamamura K, Kambe M, Miyata M, Tajima O, Ohmi Y, Yamauchi Y, Furukawa K, Furukawa K (2010) Ganglioside GD3 enhances adhesion signals and augments malignant properties of melanoma cells by recruiting integrins to glycolipid-enriched microdomains. *J Biol Chem* 285: 27213–27223

Papanikou E, Glick BS (2014) Golgi compartmentation and identity. *Curr Opin Cell Biol* 29: 74–81

Park SY, Kwak CY, Shayman JA, Kim JH (2012) Globoside promotes activation of ERK by interaction with the epidermal growth factor receptor. *Biochim Biophys Acta* 1820: 1141–1148

Pedelacq JD, Cabantous S, Tran T, Terwilliger TC, Waldo GS (2006) Engineering and characterization of a superfolder green fluorescent protein. *Nat Biotechnol* 24: 79–88

Pothukuchi P, Agliarulo I, Russo D, Rizzo R, Russo F, Parashuraman S (2019) Translation of genome to glycome: role of the Golgi apparatus. *FEBS Lett* 593: 2390–2411

Rahajeng J, Kuna RS, Makowski SL, Tran TTT, Buschman MD, Li S, Cheng N, Ng MM, Field SJ (2019) Efficient Golgi forward trafficking requires GOLPH3-Driven, PI4P-dependent membrane curvature. *Dev Cell* 50: 573–585

Reynolds CP, Maurer BJ, Kolesnick RN (2004) Ceramide synthesis and metabolism as a target for cancer therapy. *Cancer Lett* 206: 169–180

Rizzo R, Parashuraman S, Mirabelli P, Puri C, Lucocq J, Luini A (2013) The dynamics of engineered resident proteins in the mammalian Golgi complex relies on cisternal maturation. *J Cell Biol* 201: 1027–1036

Rizzo R, Parashuraman S, D'Angelo G, Luini A (2017) GOLPH3 and oncogenesis: What is the molecular link? *Tissue Cell* 49: 170–174

Russo D, Della Ragione F, Rizzo R, Sugiyama E, Scalabri F, Hori K, Capasso S, Sticco L, Fioriniello S, De Gregorio R *et al* (2018) Glycosphingolipid metabolic reprogramming drives neural differentiation. *EMBO J* 37: e97674

Russo D, Parashuraman S, D'Angelo G (2016) Glycosphingolipid-protein interaction in signal transduction. *Int J Mol Sci* 17: 1732

Schmitz KR, Liu J, Li S, Setty TG, Wood CS, Burd CG, Ferguson KM (2008) Golgi localization of glycosyltransferases requires a Vps74p oligomer. *Dev Cell* 14: 523–534

Scott KL, Chin L (2010) Signaling from the Golgi: mechanisms and models for Golgi phosphoprotein 3-mediated oncogenesis. *Clin Cancer Res* 16: 2229–2234

Scott KL, Kabbarah O, Liang MC, Ivanova E, Anagnostou V, Wu J, Dhakal S, Wu M, Chen S, Feinberg T *et al* (2009) GOLPH3 modulates mTOR signalling and rapamycin sensitivity in cancer. *Nature* 459: 1085–1090

Scotto L, Narayan G, Nandula SV, Arias-Pulido H, Subramaniyam S, Schneider A, Kaufmann AM, Wright JD, Pothuri B, Mansukhani M *et al* (2008) Identification of copy number gain and overexpressed genes on chromosome arm 20q by an integrative genomic approach in cervical cancer: potential role in progression. *Genes Chromosomes Cancer* 47: 755–765

Shimobayashi M, Hall MN (2014) Making new contacts: the mTOR network in metabolism and signalling crosstalk. *Nat Rev Mol Cell Biol* 15: 155–162

Steelant WF, Kawakami Y, Ito A, Handa K, Bruyneel EA, Mareel M, Hakomori S (2002) Monosialyl-Gb5 organized with cSrc and FAK in GEM of human breast carcinoma MCF-7 cells defines their invasive properties. *FEBS Lett* 531: 93–98

Sweet RW, Yokoyama S, Kamata T, Feramisco JR, Rosenberg M, Gross M (1984) The product of ras is a GTPase and the T24 oncogenic mutant is deficient in this activity. *Nature* 311: 273–275

Tan X, Banerjee P, Pham EA, Rutaganira FUN, Basu K, Bota-Rabassedas N, Guo HF, Grzeskowiak CL, Liu X, Yu J *et al* (2020) PI4KIIIbeta is a therapeutic target in chromosome 1q-amplified lung adenocarcinoma. *Sci Transl Med* 12: eaax3772

Tang S, Yang R, Zhou X, Pan H, Liu J (2018) Expression of GOLPH3 in patients with non-small cell lung cancer and xenografts models. *Oncol Lett* 15: 7555–7562

Tang W, Han M, Ruan B, Jin W, Lou J, Yuan X, Chen D, Chen Y, Shin VY, Jin H *et al* (2016) Overexpression of GOLPH3 is associated with poor survival in Non-small-cell lung cancer. *Am J Transl Res* 8: 1756–1762

Tang W, Li M, Qi X, Li J (2020) beta1,4-galactosyltransferase V modulates breast cancer stem cells through wnt/beta-catenin signaling pathway. *Cancer Res Treat* 52: 1084–1102

Trucco A, Polishchuk RS, Martella O, Di Pentima A, Fusella A, Di Giandomenico D, San Pietro E, Beznoussenko GV, Polishchuk EV, Baldassarre M *et al* (2004) Secretory traffic triggers the formation of tubular continuities across Golgi sub-compartments. *Nat Cell Biol* 6: 1071–1081

Tu L, Tai WC, Chen L, Banfield DK (2008) Signal-mediated dynamic retention of glycosyltransferases in the Golgi. *Science* 321: 404–407

Wang D, Zhu ZZ, Jiang H, Zhu J, Cong WM, Wen BJ, He SQ, Liu SF (2015) Multiple genes identified as targets for 20q13.12-13.33 gain contributing to unfavorable clinical outcomes in patients with hepatocellular carcinoma. *Hepatol Int* 9: 438–446

Wang H-l, Zhang Z-LJCB, Biophysics (2014) Analysis of the relationship between ultrasound of breast cancer DOT-SDI and the expression of MVD, VEGF and HIF-1α. *Cell Biochem Biophys* 70: 205–208

Wang P, Ye Z, Banfield DK (2020) A novel mechanism for the retention of Golgi membrane proteins mediated by the Bre5p/Ubp3p deubiquitinase complex. *Mol Biol Cell* 31: 2139–2155

Wegner MS, Schomel N, Gruber L, Ortel SB, Kjellberg MA, Mattjus P, Kurz J, Trautmann S, Peng B, Wegner M *et al* (2018) UDP-glucose ceramide glucosyltransferase activates AKT, promoted proliferation, and doxorubicin resistance in breast cancer cells. *Cell Mol Life Sci* 75: 3393–3410

Willett R, Ungar D, Lupashin V (2013) The Golgi puppet master: COG complex at center stage of membrane trafficking interactions. *Histochem Cell Biol* 140: 271–283

Witkos TM, Chan WL, Joensuu M, Rhiel M, Pallister E, Thomas-Oates J, Mould AP, Mironov AA, Biot C, Guerardel Y *et al* (2019) GORAB scaffolds COPI at the trans-Golgi for efficient enzyme recycling and correct protein glycosylation. *Nat Commun* 10: 127

Wong M, Munro S (2014) Membrane trafficking. The specificity of vesicle traffic to the Golgi is encoded in the golgin coiled-coil proteins. *Science* 346: 1256898

Wood CS, Hung CS, Huoh YS, Mousley CJ, Stefan CJ, Bankaitis V, Ferguson KM, Burd CG (2012) Local control of phosphatidylinositol 4-phosphate signaling in the Golgi apparatus by Vps74 and Sac1 phosphoinositide phosphatase. *Mol Biol Cell* 23: 2527–2536

Wood CS, Schmitz KR, Bessman NJ, Setty TG, Ferguson KM, Burd CG (2009) PtdIns4P recognition by Vps74/GOLPH3 links PtdIns 4-kinase signaling to retrograde Golgi trafficking. *J Cell Biol* 187: 967–975

Xie Z, Hur SK, Zhao L, Abrams CS, Bankaitis VA (2018) A golgi lipid signaling pathway controls apical golgi distribution and cell polarity during neurogenesis. *Dev Cell* 44: 725–740

Yamaji T, Hanada K (2014) Establishment of HeLa cell mutants deficient in sphingolipid-related genes using TALENs. *PLoS One* 9: e88124

Yoshimori T, Yamamoto A, Moriyama Y, Futai M, Tashiro Y (1991) Bafilomycin A1, a specific inhibitor of vacuolar-type H(+)-ATPase, inhibits acidification and protein degradation in lysosomes of cultured cells. *J Biol Chem* 266: 17707–17712

Zeng Z, Lin H, Zhao X, Liu G, Wang X, Xu R, Chen K, Li J, Song L (2012) Overexpression of GOLPH3 promotes proliferation and tumorigenicity in breast cancer via suppression of the FOXO1 transcription factor. *Clin Cancer Res* 18: 4059–4069

Zhao SB, Suda Y, Nakanishi H, Wang N, Yoko OT, Gao XD, Fujita M (2019) Yeast Dop1 is required for glycosyltransferase retrieval from the trans-Golgi network. *Biochim Biophys Acta* 1863: 1147–1157